Table 1.7.3.9. *Field-tensor components specifically nil in the principal planes of uniaxial and biaxial crystals for three-wave and four-wave interactions* $(i, j, k) = x, y$ or z.

Configurations of polarization	Nil field-tensor components		
	(xy) plane	(xz) plane	(yz) plane
eoo	$F_{xjk} = 0$; $F_{yjk} = 0$	$F_{ixk} = F_{ijx} = 0$ $F_{yjk} = 0$	$F_{iyk} = F_{ijy} = 0$ $F_{xjk} = 0$
oee	$F_{ixk} = F_{ijx} = 0$ $F_{iyk} = F_{ijy} = 0$	$F_{iyk} = F_{ijy} = 0$ $F_{xik} = 0$	$F_{ixk} = F_{ijx} = 0$ $F_{yjk} = 0$
eooo	$F_{xjkl} = 0$; $F_{yjkl} = 0$	$F_{ixkl} = F_{ijxl} = F_{ijkx} = 0$ $F_{yjkl} = 0$	$F_{iykl} = F_{ijyl} = F_{ijky} = 0$ $F_{xjkl} = 0$
oeee	$F_{ixkl} = F_{ijxl} = F_{ijkx} = 0$ $F_{iykl} = F_{ijyl} = F_{ijky} = 0$	$F_{iykl} = F_{ijyl} = F_{ijky} = 0$ $F_{xjkl} = 0$	$F_{ixkl} = F_{ijxl} = F_{ijkx} = 0$ $F_{yjkl} = 0$
ooee	$F_{ijxl} = F_{ijkx} = 0$ $F_{ijyl} = F_{ijky} = 0$	$F_{xjkl} = F_{ixkl} = 0$ $F_{ijyl} = F_{ijky} = 0$	$F_{yjkl} = F_{iykl} = 0$ $F_{ijxl} = F_{ijkx} = 0$

and configurations of polarization: D_4 and D_6 for $2o.e$, C_{4v} and C_{6v} for $2e.o$, D_6, D_{6h}, D_{3h} and C_{6v} for $3o.e$ and $3e.o$. Thus, even if phase-matching directions exist, the effective coefficient in these situations is nil, which forbids the interactions considered (Boulanger & Marnier, 1991; Boulanger *et al.*, 1993). The number of forbidden crystal classes is greater under the Kleinman approximation. The forbidden crystal classes have been determined for the particular case of third harmonic generation assuming Kleinman conjecture and without consideration of the field tensor (Midwinter & Warner, 1965).

1.7.3.2.4.3. *Biaxial class*

The symmetry of the biaxial field tensors is the same as for the uniaxial class, though only for a propagation in the principal planes xz and yz; the associated matrix representations are given in Tables 1.7.3.7 and 1.7.3.8, and the nil components are listed in Table 1.7.3.9. Because of the change of optic sign from either side of the optic axis, the field tensors of the interactions for which the phase-matching cone joins areas b and a or a and c, given in Fig. 1.7.3.5, change from one area to another: for example, the field tensor (*eoee*) becomes an (*oeoo*) and so the solicited components of the electric susceptibility tensor are not the same.

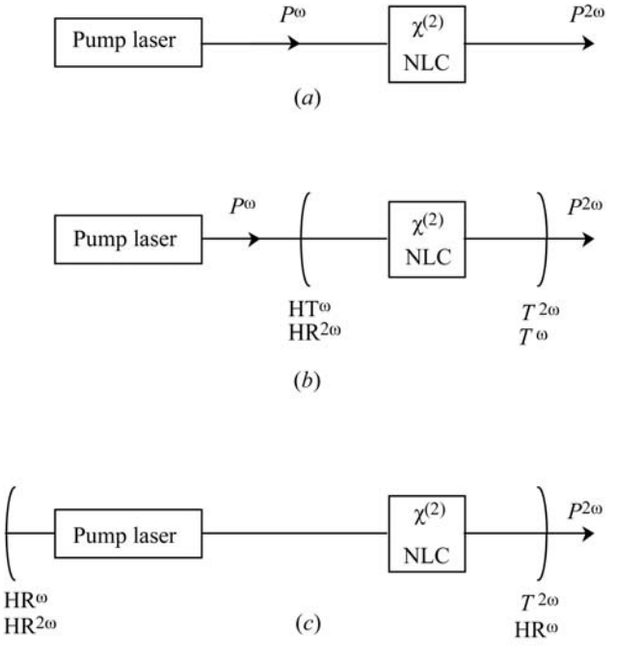

Fig. 1.7.3.6. Schematic configurations for second harmonic generation. (*a*) Non-resonant SHG; (*b*) external resonant SHG: the resonant wave may either be the fundamental or the harmonic one; (*c*) internal resonant SHG. $P^{\omega,2\omega}$ are the fundamental and harmonic powers; HT^{ω} and $HR^{\omega,2\omega}$ are the high-transmission and high-reflection mirrors at ω or 2ω and $T^{\omega,2\omega}$ are the transmission coefficients of the output mirror at ω or 2ω. NLC is the nonlinear crystal with a nonzero $\chi^{(2)}$.

The nonzero field-tensor components for a propagation in the xy plane of a biaxial crystal are: F_{zxx}, F_{zyy}, $F_{zxy} \neq F_{zyx}$ for (*eoo*); F_{xzz}, F_{yzz} for (*oee*); F_{zxxx}, F_{zyyy}, $F_{zxyy} \neq F_{zyxy} \neq F_{zyyx}$, $F_{zxxy} \neq F_{zxyx} \neq F_{zyxx}$ for (*eooo*); F_{xzzz}, F_{yzzz} for (*oeee*); $F_{xyzz} \neq F_{yxzz}$, F_{xxzz}, F_{yyzz} for (*ooee*). The nonzero components for the other configurations of polarization are obtained by the associated permutations of the Cartesian indices and the corresponding polarizations.

The field tensors are not symmetric for a propagation out of the principal planes in the general case where all the frequencies are different: in this case there are 27 independent components for the three-wave interactions and 81 for the four-wave interactions, and so all the electric susceptibility tensor components are solicited.

As phase matching imposes the directions of the electric fields of the interacting waves, it also determines the field tensor and hence the effective coefficient. Thus there is no possibility of choice of the $\chi^{(2)}$ coefficients, since a given type of phase matching is considered. In general, the largest coefficients of polar crystals, *i.e.* χ_{zzz}, are implicated at a very low level when phase matching is achieved, because the corresponding field tensor, *i.e.* F_{zzz}, is often weak (Boulanger *et al.*, 1997). In contrast, QPM authorizes the coupling between three waves polarized along the z axis, which leads to an effective coefficient which is purely χ_{zzz}, *i.e.* $\chi_{\rm eff} = (2/\pi)\chi_{zzz}$, where the numerical factor comes from the periodic character of the rectangular function of modulation (Fejer *et al.*, 1992).

1.7.3.3. *Integration of the propagation equations*

1.7.3.3.1. *Spatial and temporal profiles*

The resolution of the coupled equations (1.7.3.22) or (1.7.3.24) over the crystal length L leads to the electric field amplitude $E_i(X, Y, L)$ of each interacting wave. The general solutions are Jacobian elliptic functions (Armstrong *et al.*, 1962; Fève, Boulanger & Douady, 2002). The integration of the systems is simplified for cases where one or several beams are held constant, which is called the undepleted pump approximation. We consider mainly this kind of situation here. The power of each interacting wave is calculated by integrating the intensity over the cross section of each beam according to (1.7.3.8). For our main purpose, we consider the simple case of plane-wave beams with two kinds of transverse profile:

$$\begin{aligned} &\mathbf{E}(X, Y, Z) = \mathbf{e}E_o(Z) \quad \text{for } (X, Y) \in [-w_o, +w_o] \\ &\mathbf{E}(X, Y, Z) = 0 \quad \text{elsewhere} \end{aligned} \tag{1.7.3.36}$$

for a flat distribution over a radius w_o;

$$\mathbf{E}(X, Y, Z) = \mathbf{e}E_o(Z)\exp[-(X^2 + Y^2)/w_o^2] \tag{1.7.3.37}$$

for a Gaussian distribution, where w_o is the radius at $(1/e)$ of the electric field and so at $(1/e^2)$ of the intensity.

The associated powers are calculated according to (1.7.3.8), which leads to

$$P(L) = m(n/2)(\varepsilon_o/\mu_o)^{1/2}|E_o|^2\pi w_o^2 \tag{1.7.3.38}$$

where $m = 1$ for a flat distribution and $m = 1/2$ for a Gaussian profile.

The nonlinear interaction is characterized by the conversion efficiency, which is defined as the ratio of the generated power to the power of one or several incident beams, according to the different kinds of interactions.

For pulsed beams, it is necessary to consider the temporal shape, usually Gaussian:

$$P(t) = P_c \exp(-2t^2/\tau^2) \tag{1.7.3.39}$$

where P_c is the peak power and τ the half $(1/e^2)$ width.

For a repetition rate f (s^{-1}), the average power $\tilde{P}$ is then given by

$$\tilde{P} = P_c \tau f (\pi/2)^{1/2} = \tilde{E}f \tag{1.7.3.40}$$

where $\tilde{E}$ is the energy per Gaussian pulse.

When the pulse shape is not well defined, it is suitable to consider the energies per pulse of the incident and generated waves for the definition of the conversion efficiency.

The interactions studied here are sum-frequency generation (SFG), including second harmonic generation (SHG: $\omega + \omega = 2\omega$), cascading third harmonic generation (THG: $\omega + 2\omega = 3\omega$) and direct third harmonic generation (THG: $\omega + \omega + \omega = 3\omega$). The difference-frequency generation (DFG) is also considered, including optical parametric amplification (OPA) and oscillation (OPO).

We choose to analyse in detail the different parameters relative to conversion efficiency (figure of merit, acceptance bandwidths, walk-off effect *etc.*) for SHG, which is the prototypical second-order nonlinear interaction. This discussion will be valid for the other nonlinear processes of frequency generation which will be considered later.

1.7.3.3.2. *Second harmonic generation (SHG)*

According to Table 1.7.3.1, there are two types of phase matching for SHG: type I and type II (equivalent to type III).

The fundamental waves at ω define the pump. Two situations are classically distinguished: the undepleted pump approximation, when the power conversion efficiency is sufficiently low to consider the fundamental power to be undepleted, and the depleted case for higher efficiency. There are different ways to realize SHG, as shown in Fig. 1.7.3.6: the simplest one is non-resonant SHG, outside the laser cavity; other ways are external or internal resonant cavity SHG, which allow an enhancement of the single-pass efficiency conversion.

1.7.3.3.2.1. *Non-resonant SHG with undepleted pump in the parallel-beam limit with a Gaussian transverse profile*

We first consider the case where the crystal length is short enough to be located in the near-field region of the laser beam where the parallel-beam limit is a good approximation. We make another simplification by considering a propagation along a principal axis of the index surface: then the walk-off angle of each interacting wave is nil so that the three waves have the same coordinate system (X, Y, Z).

The integration of equations (1.7.3.22) over the crystal length Z in the undepleted pump approximation, *i.e.* $\partial E_1^\omega(X, Y, Z)/\partial Z = \partial E_2^\omega(X, Y, Z)/\partial Z = 0$, with $E_3^{2\omega}(X, Y, 0) = 0$, leads to

$$|E_3^{2\omega}(X, Y, L)|^2 = \{K_3^{2\omega}[\varepsilon_o \chi_{\text{eff}}^{(2)}]\}^2 |E_1^\omega(X, Y, 0)E_2^\omega(X, Y, 0)|^2 \times L^2 \sin c^2[(\Delta k \cdot L)/2]. \tag{1.7.3.41}$$

(1.7.3.41) implies a Gaussian transversal profile for $|E_3^{2\omega}(X, Y, L)|$ if $|E_1^\omega(X, Y, 0)|$ and $|E_2^\omega(X, Y, 0)|$ are Gaussian. The three beam radii are related by $(1/w_{o3}^2) = (1/w_{o1}^2) + (1/w_{o2}^2)$, so if we assume that the two fundamental beams have the same radius w_o^ω, which is not an approximation for type I, then $w_o^{2\omega} = [w_o^\omega/(2^{1/2})]$. Two incident beams with a flat distribution of radius w_o^ω lead to the generation of a flat harmonic beam with the same radius $w_o^{2\omega} = w_o^\omega$.

The integration of (1.7.3.41) according to (1.7.3.36)–(1.7.3.38) for a Gaussian profile gives in the SI system

$$P^{2\omega}(L) = BP_1^\omega(0)P_2^\omega(0)\frac{L^2}{w_o^2}\sin c^2\left(\frac{\Delta k \cdot L}{2}\right)$$
$$B = \frac{32\pi}{\varepsilon_o c}\frac{2N-1}{N}\frac{d_{\text{eff}}^2}{\lambda_\omega^2}\frac{T_3^{2\omega}T_1^\omega T_2^\omega}{n_3^{2\omega}n_1^\omega n_2^\omega}, \quad (\text{W}^{-1}) \tag{1.7.3.42}$$

where $c = 3 \times 10^8$ m s^{-1}, $\varepsilon_o = 8.854 \times 10^{-12}$ A s V^{-1} m^{-1} and so $(32\pi/\varepsilon_o c) = 37.85 \times 10^3$ V A^{-1}. L (m) is the crystal length in the direction of propagation. $\Delta k = k_3^{2\omega} - k_1^\omega - k_2^\omega$ is the phase mismatch. $n_3^{2\omega}$, n_1^ω and n_2^ω are the refractive indices at the harmonic and fundamental wavelengths $\lambda_{2\omega}$ and λ_ω (μm): for the phase-matching case, $\Delta k = 0$, $n_3^{2\omega} = n^-(2\omega)$, $n_1^\omega = n_2^\omega = n^+(\omega)$ for type I (the two incident fundamental beams have the same polarization contained in Π^+, with the harmonic polarization contained in Π^-) and $n_1^\omega = n^+(\omega) \neq n_2^\omega = n^-(\omega)$ for type II (the two solicited eigen modes at the fundamental wavelength are in Π^+ and Π^-, with the harmonic polarization contained in Π^-). $T_3^{2\omega}$, T_1^ω and T_2^ω are the transmission coefficients given by $T_i = 4n_i/(n_i + 1)^2$. d_{eff} (pm V^{-1}) $= (1/2)\chi_{\text{eff}} = (1/2)[F^{(2)} \cdot \chi^{(2)}]$ is the effective coefficient given by (1.7.3.30) and (1.7.3.31). $P_1^\omega(0)$ and $P_2^\omega(0)$ are the two incident fundamental powers, which are not necessarily equal for type II; for type I we have obviously $P_1^\omega(0) = P_2^\omega(0) = (P_{\text{tot}}^\omega/2)$. N is the number of independently oscillating modes at the fundamental wavelength: every longitudinal mode at the harmonic pulsation can be generated by many combinations of two fundamental modes; the $(2N-1)/N$ factor takes into account the fluctuations between these longitudinal modes (Bloembergen, 1963).

The powers in (1.7.3.42) are instantaneous powers $P(t)$.

The second harmonic (SH) conversion efficiency, η_{SHG}, is usually defined as the ratio of peak powers $P_c^{2\omega}(L)/P_{c,\text{tot}}^\omega(0)$, or as the ratio of the pulse total energy $\tilde{E}^{2\omega}(L)/\tilde{E}_{\text{tot}}^\omega(0)$. For Gaussian temporal profiles, the SH $(1/e^2)$ pulse duration $\tau_{2\omega}$ is equal to $\tau_\omega/(2^{1/2})$, because $P_{2\omega}$ is proportional to P_ω^2, and so, according to (1.7.3.40), the pulse average energy conversion efficiency is $1/(2^{1/2})$ smaller than the peak power conversion efficiency given by (1.7.3.42). Note that the pulse total energy conversion efficiency is equivalent to the average power conversion efficiency $\tilde{P}^{2\omega}(L)/\tilde{P}_{\text{tot}}^\omega(0)$, with $\tilde{P} = \tilde{E} \cdot f$ where f is the repetition rate.

Formula (1.7.3.42) shows the importance of the contribution of the linear optical properties to the nonlinear process. Indeed, the field tensor $F^{(2)}$, the transmission coefficients T_i and the phase mismatch Δk only depend on the refractive indices in the direction of propagation considered.

(i) *Figure of merit*.

The contribution of $F^{(2)}$ was discussed previously, where it was shown that the field tensor is nil in particular directions of propagation or everywhere for particular crystal classes and configurations of polarization (even if the nonlinearity $\chi^{(2)}$ is high).

The field tensor $F^{(2)}$ of SHG can be written with the contracted notation of $d^{(2)}$; according to Table 1.7.3.1 and to the contraction

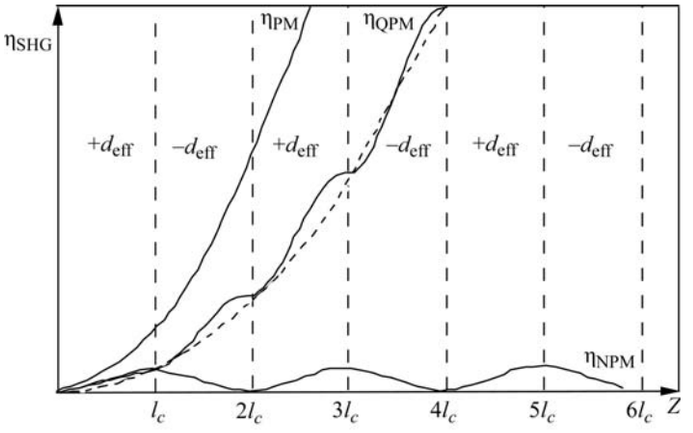

Fig. 1.7.3.7. Spatial growth evolution of second harmonic conversion efficiency, η_{SHG}, for non phase matching (NPM), $\Delta k \neq 0$, and phase matching (PM), $\Delta k = 0$, in a 'continuous' crystal, and for quasi phase matching (QPM) in a periodic structure. The dashed curve corresponds to $(4/\pi^2)\eta_{PM}(Z)$ where η_{PM} is the conversion efficiency of the phase-matched SHG. $l_c = \pi/\Delta k$ is the coherence length.

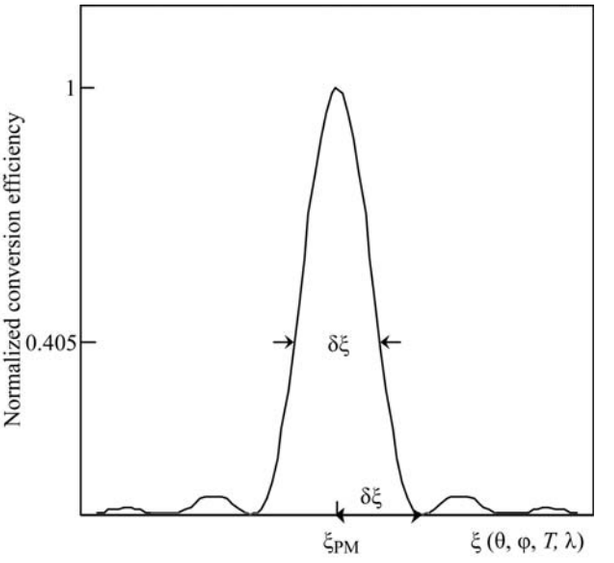

Fig. 1.7.3.8. Conversion efficiency evolution as a function of ξ for a given crystal length. ξ denotes the angle (θ or φ), the temperature (T) or the wavelength (λ). ξ_{PM} represents the parameter allowing phase matching.

conventions given in Section 1.7.2.2, the contracted field-tensor components for the phase-matched SHG are

$$\begin{aligned}
F_{i1} &= \mathbf{e}_i^-(2\omega)[\mathbf{e}_x^+(\omega)]^2 \\
F_{i2} &= \mathbf{e}_i^-(2\omega)[\mathbf{e}_y^+(\omega)]^2 \\
F_{i3} &= \mathbf{e}_i^-(2\omega)[\mathbf{e}_z^+(\omega)]^2 \\
F_{i4} &= 2\mathbf{e}_i^-(2\omega)\mathbf{e}_y^+(\omega)\mathbf{e}_z^+(\omega) \\
F_{i5} &= 2\mathbf{e}_i^-(2\omega)\mathbf{e}_x^+(\omega)\mathbf{e}_z^+(\omega) \\
F_{i6} &= 2\mathbf{e}_i^-(2\omega)\mathbf{e}_x^+(\omega)\mathbf{e}_y^+(\omega)
\end{aligned}$$

for type I and

$$\begin{aligned}
F_{i1} &= \mathbf{e}_i^-(2\omega)\mathbf{e}_x^+(\omega)\mathbf{e}_x^-(\omega) \\
F_{i2} &= \mathbf{e}_i^-(2\omega)\mathbf{e}_y^+(\omega)\mathbf{e}_y^-(\omega) \\
F_{i3} &= \mathbf{e}_i^-(2\omega)\mathbf{e}_z^+(\omega)\mathbf{e}_z^-(\omega) \\
F_{i4} &= \mathbf{e}_i^-(2\omega)[\mathbf{e}_y^+(\omega)\mathbf{e}_z^-(\omega) + \mathbf{e}_y^-(\omega)\mathbf{e}_z^+(\omega)] \\
F_{i5} &= \mathbf{e}_i^-(2\omega)[\mathbf{e}_x^+(\omega)\mathbf{e}_z^-(\omega) + \mathbf{e}_x^-(\omega)\mathbf{e}_z^+(\omega)] \\
F_{i6} &= \mathbf{e}_i^-(2\omega)[\mathbf{e}_x^+(\omega)\mathbf{e}_y^-(\omega) + \mathbf{e}_x^-(\omega)\mathbf{e}_y^+(\omega)]
\end{aligned}$$

for type II, with $i = (1, 2, 3)$ for F_{ij}, corresponding to $i = (x, y, z)$ for $\mathbf{e}_i^-(2\omega)$.

The ratio $d_{eff}^2/n_3^{2\omega}n_1^{\omega}n_2^{\omega}$ in formula (1.7.3.42) is called the figure of merit of the direction considered. The effective coefficient is given in Section 1.7.5 for the main nonlinear crystals and for chosen SHG wavelengths.

(ii) *Effect of the phase mismatch.*

The interference function $\sin c^2(\Delta kL/2)$ is a maximum and equal to unity only for $\Delta k = 0$, which defines the phase-matching condition. Fig. 1.7.3.7 shows the effect of the phase mismatch on the growth of second harmonic conversion efficiency, η_{SHG}, with interaction distance Z.

The conversion efficiency has a Z^2 dependence in the case of phase matching. The harmonic power oscillates around Z^2 for quasi phase matching, but is reduced by a factor of $4/\pi^2$ compared with that of phase-matched interaction (Fejer *et al.*, 1992).

An SHG phase-matching direction $(\theta_{PM}, \varphi_{PM})$ for given fundamental wavelength (λ_{PM}) and type of interaction, I or II, is defined at a given temperature (T_{PM}). It is important to consider the effect of deviation of Δk from 0 due to variations of angles $(\theta_{PM} \pm d\theta, \varphi_{PM} \pm d\varphi)$, of temperature $(T_{PM} \pm dT)$ and of wavelength $(\lambda_{PM} \pm d\lambda)$ on the conversion efficiency. The quantities that characterize these effects are the acceptance bandwidths $\delta\xi$ $(\xi = \theta, \varphi, T, \lambda)$, usually defined as the deviation from the phase-matching value ξ_{PM} leading to a phase-mismatch variation Δk from 0 to $2\pi/L$, where L is the crystal length. Then $\delta\xi$ is also the full width of the peak efficiency curve plotted as a function of ξ at 0.405 of the maximum, as shown in Fig. 1.7.3.8.

Thus $L\delta\xi$ is a characteristic of the phase-matching direction. Small angular, thermal and spectral dispersion of the refractive indices lead to high acceptance bandwidths. The higher $L\delta\xi$, the lower is the decrease of the conversion efficiency corresponding to a given angular shift, to the heating of the crystal due to absorption or external heating, or to the spectral bandwidth of the fundamental beam.

The knowledge of the angular, thermal and spectral dispersion of the refractive indices allows an estimation of $\delta\xi$ by expanding Δk in a Taylor series about ξ_{PM}:

$$\frac{2\pi}{L} = \Delta k = \left.\frac{\partial(\Delta k)}{\partial\xi}\right|_{\xi_{PM}} \delta\xi + \frac{1}{2}\left.\frac{\partial^2(\Delta k)}{\partial\xi^2}\right|_{\xi_{PM}} (\delta\xi)^2 + \ldots . \quad (1.7.3.43)$$

When the second- and higher-order differential terms in (1.7.3.43) are negligible, the phase matching is called critical (CPM), because $L\delta\xi \simeq |2\pi/[\partial(\Delta k)/\partial\xi|_{\xi_{PM}}]|$ is small. For the particular cases where $\partial(\Delta k)/\partial\xi|_{\xi_{PM}} = 0$, $L\delta\xi = \{|4\pi L/[\partial^2(\Delta k)/\partial\xi^2|_{\xi_{PM}}]|\}^{1/2}$ is larger than the CPM acceptance and the phase matching is called non-critical (NCPM) for the parameter ξ considered.

We first consider the case of angular acceptances. In uniaxial crystals, the refractive indices do not vary in φ, leading to an infinite φ angular acceptance bandwidth. $\delta\theta$ is then the only one to consider. For directions of propagation out of the principal plane ($\theta_{PM} \neq \pi/2$), the phase matching is critical. According to the expressions of n_o and $n_e(\theta)$ given in Section 1.7.3.1, we have

(1) for type I in positive crystals, $n_e(\theta, \omega) = n_o(2\omega)$ and

$$L\delta\theta \simeq 2\pi/\{-(\omega/c)n_o^3(2\omega)[n_e^{-2}(\omega) - n_o^{-2}(\omega)]\sin 2\theta_{PM}\}; \quad (1.7.3.44)$$

(2) for type II in positive crystals, $2n_o(2\omega) = n_e(\theta, \omega) + n_o(\omega)$ and

$$L\delta\theta \simeq 2\pi/\{-(\omega/2c)[2n_o(2\omega) - n_o(\omega)]^3 \times [n_e^{-2}(\omega) - n_o^{-2}(\omega)]\sin 2\theta_{\rm PM}\}; \quad (1.7.3.45)$$

(3) for type I in negative crystals, $n_e(\theta, 2\omega) = n_o(\omega)$ and

$$L\delta\theta \simeq 2\pi/\{-(\omega/c)n_o^3(\omega)[n_o^{-2}(2\omega) - n_e^{-2}(2\omega)]\sin 2\theta_{\rm PM}\}; \quad (1.7.3.46)$$

(4) for type II in negative crystals, $2n_e(\theta, 2\omega) = n_e(\theta, \omega) + n_o(\omega)$ and

$$L\delta\theta \simeq \big|2\pi/\{-(\omega/c)n_e^3(\theta, 2\omega)[n_e^{-2}(2\omega) - n_o^{-2}(2\omega)]\sin 2\theta_{\rm PM} + (\omega/2c)n_e^3(\theta, \omega)[n_e^{-2}(\omega) - n_o^{-2}(\omega)]\sin 2\theta_{\rm PM}\}\big|. \quad (1.7.3.47)$$

CPM acceptance bandwidths are small, typically about one mrad cm, as shown in Section 1.7.5 for the classical nonlinear crystals.

When $\theta_{\rm PM} = \pi/2$, $\partial\Delta k/\partial\theta = 0$ and the phase matching is non-critical:

(1) for type I in positive crystals, $n_e(\omega) = n_o(2\omega)$ and

$$L\delta\theta \simeq \big(2\pi L/\{-(\omega/c)n_o^3(2\omega)[n_e^{-2}(\omega) - n_o^{-2}(\omega)]\}\big)^{1/2}; \quad (1.7.3.48)$$

(2) for type II in positive crystals, $2n_o(2\omega) = n_e(\omega) + n_o(\omega)$ and

$$L\delta\theta \simeq \big(2\pi L/\{-(\omega/2c)n_e^3(\omega)[n_e^{-2}(\omega) - n_o^{-2}(\omega)]\}\big)^{1/2}; \quad (1.7.3.49)$$

(3) for type I in negative crystals, $n_o(\omega) = n_e(2\omega)$ and

$$L\delta\theta \simeq \big(2\pi L/\{(\omega/c)n_o^3(\omega)[n_e^{-2}(2\omega) - n_o^{-2}(2\omega)]\}\big)^{1/2}; \quad (1.7.3.50)$$

(4) for type II in negative crystals, $2n_e(2\omega) = n_e(\omega) + n_o(\omega)$ and

$$L\delta\theta \simeq \big(|2\pi L/\{-(\omega/c)n_e^3(2\omega)[n_e^{-2}(2\omega) - n_o^{-2}(2\omega)] + (\omega/2c)n_e^3(\omega)[n_e^{-2}(\omega) - n_o^{-2}(\omega)]\}|\big)^{1/2}. \quad (1.7.3.51)$$

Values of NCPM acceptance bandwidths are given in Section 1.7.5 for the usual crystals. From the previous expressions for CPM and NCPM angular acceptances, it appears that the angular bandwidth is all the smaller since the birefringence is high.

The situation is obviously more complex in the case of biaxial crystals. The φ acceptance bandwidth is not infinite, leading to a smaller anisotropy of the angular acceptance in comparison with uniaxial crystals. The expressions of the θ and φ acceptance bandwidths have the same form as for the uniaxial class only in the principal planes. The phase matching is critical (CPM) for all directions of propagation out of the principal axes x, y and z: in this case, the mismatch Δk is a linear function of small angular deviations from the phase-matching direction as for uniaxial crystals. There exist six possibilities of NCPM for SHG, types I and II along the three principal axes, corresponding to twelve different index conditions (Hobden, 1967):

(1) for positive biaxial crystals

$$\begin{array}{ll} \text{Type I } (x) & n_{2\omega}^y = n_\omega^z \\ \text{Type I } (y) & n_{2\omega}^x = n_\omega^z \\ \text{Type I } (z) & n_{2\omega}^x = n_\omega^y \\ \text{Type II } (x) & n_{2\omega}^y = \tfrac{1}{2}(n_\omega^y + n_\omega^z) \\ \text{Type II } (y) & n_{2\omega}^x = \tfrac{1}{2}(n_\omega^x + n_\omega^z) \\ \text{Type II } (z) & n_{2\omega}^x = \tfrac{1}{2}(n_\omega^x + n_\omega^y); \end{array} \quad (1.7.3.52)$$

(2) for negative biaxial crystals

$$\begin{array}{ll} \text{Type I } (x) & n_{2\omega}^z = n_\omega^y \\ \text{Type I } (y) & n_{2\omega}^z = n_\omega^x \\ \text{Type I } (z) & n_{2\omega}^y = n_\omega^x \\ \text{Type II } (x) & n_{2\omega}^z = \tfrac{1}{2}(n_\omega^y + n_\omega^z) \\ \text{Type II } (y) & n_{2\omega}^z = \tfrac{1}{2}(n_\omega^x + n_\omega^z) \\ \text{Type II } (z) & n_{2\omega}^y = \tfrac{1}{2}(n_\omega^x + n_\omega^y). \end{array}$$

The NCPM angular acceptances along the three principal axes of biaxial crystals can be deduced from the expressions relative to the uniaxial class by the following substitutions:

Along the x axis:

$L\delta\varphi$ (type I > 0) = (1.7.3.50) with $n_o(\omega) \to n_z(\omega)$, $n_e(2\omega) \to n_y(2\omega)$ and $n_o(2\omega) \to n_x(2\omega)$

$L\delta\theta$ (type I > 0) = (1.7.3.48) with $n_o(2\omega) \to n_y(2\omega)$, $n_e(\omega) \to n_z(\omega)$ and $n_o(\omega) \to n_x(\omega)$

$L\delta\varphi$ (type II > 0) = (1.7.3.51) with $n_e \to n_y$ and $n_o \to n_x$

$L\delta\theta$ (type II > 0) = (1.7.3.49) with $n_e(\omega) \to n_z(\omega)$ and $n_o(\omega) \to n_x(\omega)$

$L\delta\varphi$ (type I < 0) = (1.7.3.48) with $n_o(2\omega) \to n_z(2\omega)$, $n_e(\omega) \to n_x(\omega)$ and $n_o(\omega) \to n_y(\omega)$

$L\delta\theta$ (type I < 0) = (1.7.3.50) with $n_o(\omega) \to n_y(\omega)$, $n_e(2\omega) \to n_z(2\omega)$ and $n_o(2\omega) \to n_x(2\omega)$

$L\delta\varphi$ (type II < 0) = (1.7.3.49) with $n_e(\omega) \to n_x(\omega)$ and $n_o(\omega) \to n_y(\omega)$

$L\delta\theta$ (type II < 0) = (1.7.3.51) with $n_e \to n_z$ and $n_o \to n_x$.

Along the y axis:

$L\delta\varphi$ is the same as along the x axis for all interactions

$L\delta\theta$ (type I > 0) = (1.7.3.48) with $n_o(2\omega) \to n_x(2\omega)$, $n_e(\omega) \to n_z(\omega)$ and $n_o(\omega) \to n_y(\omega)$

$L\delta\theta$ (type II > 0) = (1.7.3.49) with $n_e(\omega) \to n_z(\omega)$ and $n_o(\omega) \to n_y(\omega)$

$L\delta\theta$ (type I < 0) = (1.7.3.50) with $n_o(\omega) \to n_x(\omega)$, $n_e(2\omega) \to n_z(2\omega)$ and $n_o(2\omega) \to n_y(2\omega)$

$L\delta\theta$ (type II < 0) = (1.7.3.51) with $n_e \to n_z$ and $n_o \to n_y$.

Along the z axis:

$L\delta\theta_{xz}$ (type I > 0) = (1.7.3.48) with $n_o(2\omega) \to n_y(2\omega)$, $n_e(\omega) \to n_x(\omega)$ and $n_o(\omega) \to n_z(\omega)$

$L\delta\theta_{yz}$ (type I > 0) = (1.7.3.48) with $n_o(2\omega) \to n_x(2\omega)$, $n_e(\omega) \to n_y(\omega)$ and $n_o(\omega) \to n_z(\omega)$

$L\delta\theta_{xz}$ (type II > 0) = (1.7.3.49) with $n_e(\omega) \to n_x(\omega)$ and $n_o(\omega) \to n_z(\omega)$

$L\delta\theta_{yz}$ (type II > 0) = (1.7.3.49) with $n_e(\omega) \to n_y(\omega)$ and $n_o(\omega) \to n_z(\omega)$

$L\delta\theta_{xz}$ (type I < 0) = (1.7.3.50) with $n_o(\omega) \to n_y(\omega)$, $n_e(2\omega) \to n_z(2\omega)$ and $n_o(2\omega) \to n_x(2\omega)$

$L\delta\theta_{yz}$ (type I < 0) = (1.7.3.50) with $n_o(\omega) \to n_x(\omega)$, $n_e(2\omega) \to n_z(2\omega)$ and $n_o(2\omega) \to n_y(2\omega)$

$L\delta\theta_{xz}$ (type II < 0) = (1.7.3.51) with $n_e \rightarrow n_x$ and $n_o \rightarrow n_z$

$L\delta\theta_{yz}$ (type II < 0) = (1.7.3.51) with $n_e \rightarrow n_y$ and $n_o \rightarrow n_z$.

The above formulae are relative to the internal angular acceptance bandwidths. The external acceptance angles are enlarged by a factor of approximately $n(\omega)$ for type I or $[n_1(\omega) + n_2(\omega)]/2$ for type II, due to refraction at the input plane face of the crystal. The angular acceptance is an important issue connected with the accuracy of cutting of the crystal.

Temperature tuning is a possible alternative for achieving NCPM in a few materials. The corresponding temperatures for different interactions are given in Section 1.7.5.

Another alternative is to use a special non-collinear configuration known as one-beam non-critical non-collinear phase matching (OBNC): it is non-critical with respect to the phase-matching angle of one of the input beams (referred to as the non-critical beam). It has been demonstrated that the angular acceptance bandwidth for the non-critical beam is exceptionally large, for example about 50 times that for the critical beam for type-I SHG at 1.338 μm in 3-methyl-4-nitropyridine-*N*-oxide (POM) (Dou *et al.*, 1992).

The typical values of thermal acceptance bandwidth, given in Section 1.7.5, are of the order of 0.5 to 50 K cm. The thermal acceptance is an important issue for the stability of the harmonic power when the absorption at the wavelengths concerned is high or when temperature tuning is used for the achievement of angular NCPM. Typical spectral acceptance bandwidths for SHG are given in Section 1.7.5. The values are of the order of 1 nm cm, which is much larger than the linewidth of a single-frequency laser, except for some diode or for sub-picosecond lasers with a large spectral bandwidth.

Note that a degeneracy of the first-order temperature or spectral derivatives ($\partial\Delta k/\partial T|_{T_{PM}} = 0$ or $\partial\Delta k/\partial\lambda|_{\lambda_{PM}} = 0$) can occur and lead to thermal or spectral NCPM.

Consideration of the phase-matching function $\lambda_{PM} = f(\xi_{PM})$, where $\chi_{PM} = T_{PM}, \theta_{PM}, \varphi_{PM}$ or all other dispersion parameters of the refractive indices, is useful for a direct comparison of the situation of non-criticality of the phase matching relative to λ_{PM} and to the other parameters ξ_{PM}: a nil derivative of λ_{PM} with respect to ξ_{PM}, *i.e.* $d\lambda_{PM}/d\xi_{PM} = 0$ at the point $(\lambda^o_{PM}, \xi^o_{PM})$, means that the phase matching is non-critical with respect to ξ_{PM} and so strongly critical with respect to λ_{PM}, *i.e.* $d\xi_{PM}/d\lambda_{PM} = \infty$ at this point. Then, for example, an angular NCPM direction is a spectral CPM direction and the reverse is also so.

(iii) *Effect of spatial walk-off.*

The interest of the NCPM directions is increased by the fact that the walk-off angle of any wave is nil: the beam overlap is complete inside the nonlinear crystal. Under CPM, the interacting waves propagate with different walk-off angles: the conversion efficiency is then attenuated because the different Poynting vectors are not collinear and the beams do not overlap. Type I and type II are not equivalent in terms of walk-off angles. For type I, the two fundamental waves have the same polarization $\mathbf{E}^+$ and the same walk-off angle ρ^+, which is different from the harmonic one; thus the coordinate systems that are involved in equations (1.7.3.22) are $(X_1, Y_1, Z) = (X_2, Y_2, Z) = (X^+_\omega, Y^+_\omega, Z)$ and $(X_3, Y_3, Z) = (X^-_{2\omega}, Y^-_{2\omega}, Z)$. For type II, the two fundamental waves have necessarily different walk-off angles ρ^+ and ρ^-, which forbids the nonlinear interaction beyond the plane where the two fundamental beams are completely separated. In this case we have three different coordinate systems: $(X_1, Y_1, Z) = (X^+_\omega, Y^+_\omega, Z)$, $(X_2, Y_2, Z) = (X^-_\omega, Y^-_\omega, Z)$ and $(X_3, Y_3, Z) = (X^-_{2\omega}, Y^-_{2\omega}, Z)$.

The three coordinate systems are linked by the refraction angles ρ of the three waves as explained in Section 1.7.3.2.1. We consider Gaussian transverse profiles: the electric field amplitude is then given by (1.7.3.37). In these conditions, the integration of (1.7.3.22) over (X, Y, Z) by assuming $\tan\rho = \rho$, the non-depletion of the pump and, in the case of phase matching, $\Delta k = 0$ leads to the efficiency $\eta_{SHG}(L)$ given by formula (1.7.3.42) with $\sin c^2(\Delta kL/2) = 1$ and multiplied by the factor $[G(L, w_o, \rho)]/[\cos^2\rho(2\omega)]$ where $\rho(2\omega)$ is the harmonic walk-off angle and $G(L, w_o, \rho)$ is the walk-off attenuation function.

For type I, the walk-off attenuation is given by (Boyd *et al.*, 1965)

$$G_I(t) = (\pi^{1/2}/t)\,\mathrm{erf}(t) - (1/t^2)[1 - \exp(-t^2)]$$

with

$$t = (\rho L/w_o) \qquad (1.7.3.53)$$

and

$$\mathrm{erf}(x) = (2/\pi^{1/2}) \int_0^x \exp(-t^2)\,\mathrm{d}t.$$

For uniaxial crystals, $\rho = \rho^e(2\omega)$ for a $2oe$ interaction and $\rho = \rho^e(\omega)$ for a $2eo$ interaction. For the biaxial class, $\rho = \rho^e(2\omega)$ for a $2oe$ interaction and $\rho = \rho^e(\omega)$ for a $2eo$ interaction in the xz and yz planes, $\rho = \rho^o(\omega)$ for a $2oe$ interaction and $\rho = \rho^o(2\omega)$ for a $2eo$ interaction in the xy plane. For any direction of propagation not contained in the principal planes of a biaxial crystal, the fundamental and harmonic waves have nonzero walk-off angles, respectively $\rho^+(\omega)$ and $\rho^-(2\omega)$. In this case, (1.7.3.53) can be used with $\rho = |\rho^+(\omega) - \rho^-(2\omega)|$.

(*a*) For small t ($t \ll 1$), $G_I(t) \simeq 1$ and $P^{2\omega}(L) \equiv L^2$,

(*b*) For large t ($t \gg 1$), $G_I(t) \simeq (\pi^{1/2}/t)$ and so $P^{2\omega}(L) \equiv L/\rho$ according to (1.7.3.42) with $\Delta k = 0$.

For type II, we have (Mehendale & Gupta, 1988)

$$G_{II}(t) = (2/\pi^{1/2}) \int_{-\infty}^{+\infty} F^2(a, t)\,\mathrm{d}a$$

with

$$F(a, t) = (1/t)\exp(-a^2) \int_0^t \exp[-(a + \tau)^2]\,\mathrm{d}\tau \qquad (1.7.3.54)$$

and

$$a = \frac{r}{w_o} \quad \tau = \frac{\rho u}{w_o} \quad t = \frac{\rho L}{w_o}.$$

r and u are the Cartesian coordinates in the walk-off plane where u is collinear with the three wavevectors, *i.e.* the phase-matching direction.

$\rho = \rho^e(\omega)$ for (oeo) in uniaxial crystals and in the xz and yz planes of biaxial crystals. $\rho = \rho^o(\omega)$ in the xy plane of biaxial crystals for an (eoe) interaction.

For the interactions where $\rho^-(2\omega)$ and $\rho^-(\omega)$ are nonzero, we assume that they are close and contained in the same plane, which is generally the case. Then we classically take ρ to be the maximum value between $|\rho^-(2\omega) - \rho^+(\omega)|$ and $|\rho^-(\omega) - \rho^+(\omega)|$. This approximation concerns the (eoe) configuration of polarization in uniaxial crystals and for biaxial crystals in the xz and yz planes, in the xy plane for (oeo) and out of the principal planes for all the configurations of polarization.

The exact calculation of G, which takes into account the three walk-off angles, $\rho^-(\omega)$, $\rho^+(\omega)$ and $\rho^-(2\omega)$, was performed in the case where these three angles were coplanar (Asaumi, 1992). The exact calculation in the case of $KTiOPO_4$ (KTP) for type-II SHG at 1.064 μm gives the same result for $L/z_R < 1$ as for one angle defined as previously (Fève *et al.*, 1995), which includes the parallel-beam limit $L/z_R <$ 0.3–0.4: $z_R = [k(\omega)w_o^2]/2$ is the Rayleigh length of the fundamental beam inside the crystal.

(*a*) For $t \ll 1$, $G_{II}(t) \simeq 1$, leading to the L^2 dependence of $P^{2\omega}(L)$.

(*b*) For $t \gg 1$, $G_{II}(t) \simeq (t_a^2/t^2)$ with $t_a = [(2)^{1/2} \arctan(2^{1/2})]^{1/2}$, corresponding to a saturation of $P^{2\omega}(L)$ because of the walk-off between the two fundamental beams as shown in Fig. 1.7.3.9.

The saturation length, $L_{\rm sat}$, is defined as $2.3 t_a w_o/\rho$, which corresponds to the length beyond which the SHG conversion efficiency varies less than 1% from its saturation value $BP^{\omega}(0)t_a^2/\rho^2$.

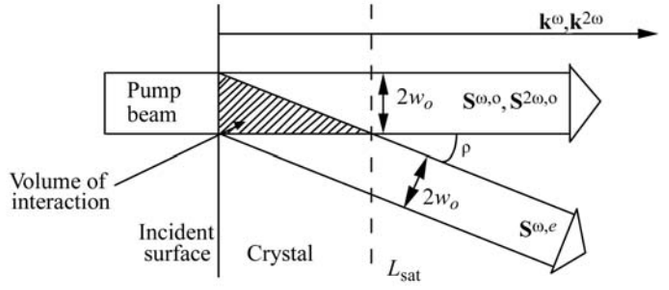

Fig. 1.7.3.9. Beam separation in the particular case of type-II (*oeo*) SHG out of the *xy* plane of a positive uniaxial crystal or in the *xz* and *yz* planes of a positive biaxial crystal. $\mathbf{S}^{\omega,o}$, $\mathbf{S}^{\omega,e}$ and $\mathbf{S}^{2\omega,o}$ are the fundamental and harmonic Poynting vectors; $\mathbf{k}^{\omega}$ and $\mathbf{k}^{2\omega}$ are the associated wavevectors collinear to the CPM direction. w_o is the fundamental beam radius and ρ is the walk-off angle. $L_{\rm sat}$ is the saturation length.

The complete splitting of the two fundamental beams does not occur for type I, making it more suitable than type II for strong focusing. The fundamental beam splitting for type II also leads to a saturation of the acceptance bandwidths $\delta\xi$ ($\xi = \theta, \varphi, T, \lambda$), which is not the case for type I (Fève *et al.*, 1995). The walk-off angles also modify the transversal distribution of the generated harmonic beam (Boyd *et al.*, 1965; Mehendale & Gupta, 1988): the profile is larger than that of the fundamental beam for type I, contrary to type II.

The walk-off can be compensated by the use of two crystals placed one behind the other, with the same length and cut in the same CPM direction (Akhmanov *et al.*, 1975): the arrangement of the second crystal is obtained from that of the first one by a π rotation around the direction of propagation or around the direction orthogonal to the direction of propagation and contained in the walk-off plane as shown in Fig. 1.7.3.10 for the particular case of type II (*oeo*) in a positive uniaxial crystal out of the *xy* plane.

The twin-crystal device is potentially valid for both types I and II. The relative sign of the effective coefficients of the twin crystals depends on the configuration of polarization, on the relative arrangement of the two crystals and on the crystal class. The interference between the waves generated in the two crystals is destructive and so cancels the SHG conversion efficiency if the two effective coefficients have opposite signs: it is always the case for certain crystal classes and configurations of polarization (Moore & Koch, 1996).

Such a tandem crystal was used, for example, with $KTiOPO_4$ (KTP) for type-II SHG at $\lambda_{\omega} = 1.3$ µm ($\rho = 2.47^{\circ}$) and $\lambda_{\omega} = 2.532$ µm ($\rho = 2.51^{\circ}$): the conversion efficiency was about 3.3 times the efficiency in a single crystal of length $2L$, where L is the length of each crystal of the twin device (Zondy *et al.*, 1994). The two crystals have to be antireflection coated or contacted in order to avoid Fresnel reflection losses.

Non-collinear phase matching is another method allowing a reduction of the walk-off, but only in the case of type II (Dou *et al.*, 1992). Fig. 1.7.3.11 illustrates the particular case of (*oeo*) type-II SHG for a propagation out of the *xy* plane of a uniaxial crystal, or in the *xz* or *yz* plane of a biaxial crystal.

In the configuration of special non-collinear phase matching, the angle between the fundamental beams inside the crystal is chosen to be equal to the walk-off angle ρ. Then the associated Poynting vectors $\mathbf{S}^{\omega,o}$ and $\mathbf{S}^{\omega,e}$ are along the same direction, while that of the generated wave deviates from them only by approximately $\rho/2$. The calculation performed in the case of special non-collinear phase matching indicates that it is possible to increase type-II SHG conversion efficiency by 17% for near-field undepleted Gaussian beams (Dou *et al.*, 1992). Another advantage of such geometry is to turn type II into a pseudo type I with respect to the walk-off,

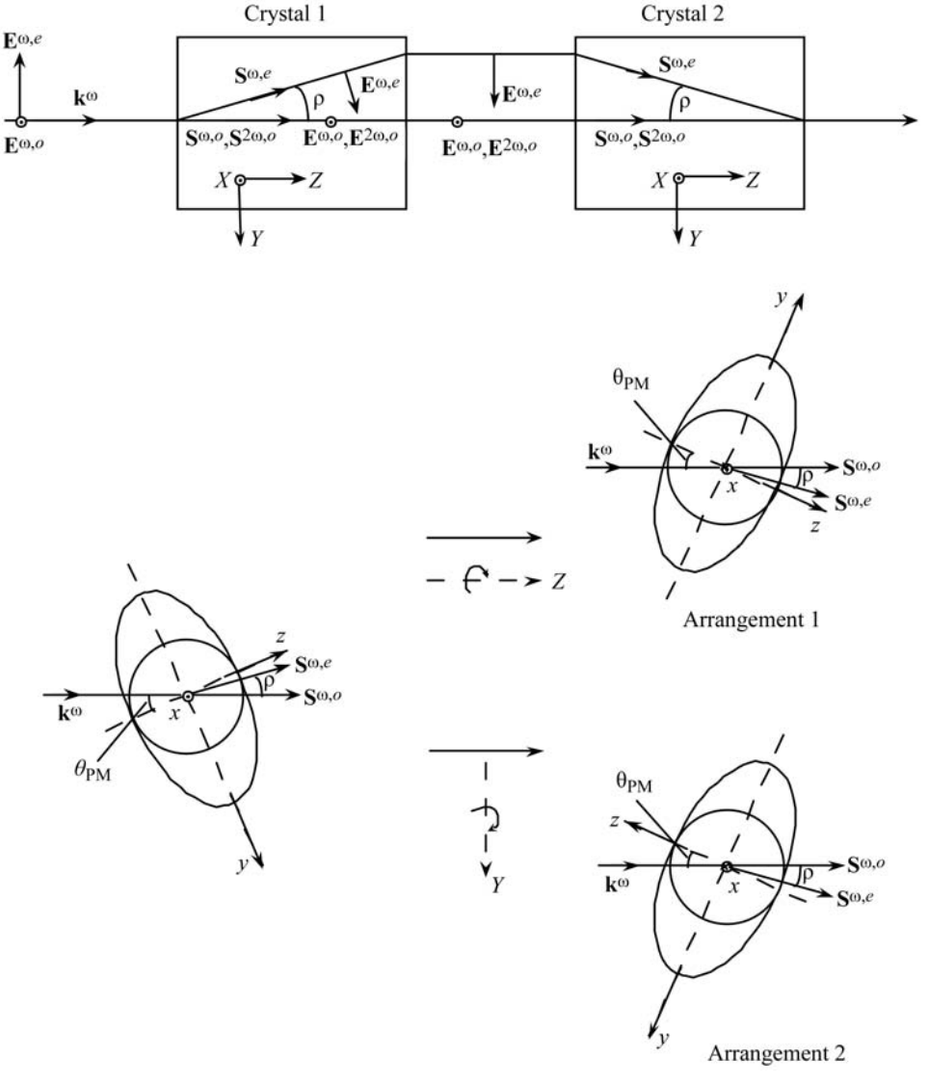

Fig. 1.7.3.10. Twin-crystal device allowing walk-off compensation for a direction of propagation $\theta_{\rm PM}$ in the *yz* plane of a positive uniaxial crystal. (X, Y, Z) is the wave frame and (x, y, z) is the optical frame. The index surface is given in the *yz* plane. $\mathbf{k}^{\omega}$ is the incident fundamental wavevector. The refracted wavevectors $\mathbf{k}^{\omega,o}$, $\mathbf{k}^{\omega,e}$ and $\mathbf{k}^{2\omega,o}$ are collinear and along $\mathbf{k}^{\omega}$. $\mathbf{S}^{\omega,o}$, $\mathbf{S}^{\omega,e}$ and $\mathbf{S}^{2\omega,o}$ are the Poynting vectors of the fundamental and harmonic waves. $\mathbf{E}^{\omega,o}$, $\mathbf{E}^{\omega,e}$ and $\mathbf{E}^{2\omega,o}$ are the electric field vectors. ρ is the walk-off angle.

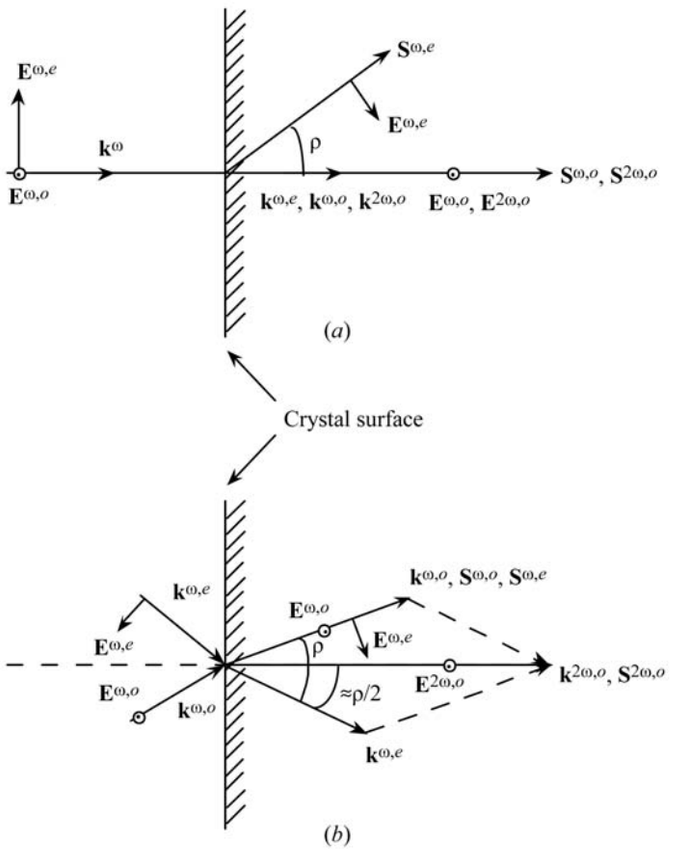

Fig. 1.7.3.11. Comparison between (*a*) collinear and (*b*) special non-collinear phase matching for (*oeo*) type-II SHG. $\mathbf{k}^{\omega,o}$, $\mathbf{k}^{\omega,e}$ and $\mathbf{k}^{2\omega,o}$ are the wavevectors, $\mathbf{S}^{\omega,o}$, $\mathbf{S}^{\omega,e}$ and $\mathbf{S}^{2\omega,o}$ are the Poynting vectors of the fundamental and harmonic waves, and $\mathbf{E}^{\omega,o}$, $\mathbf{E}^{\omega,e}$ and $\mathbf{E}^{2\omega,o}$ are the electric field vectors; ρ is the walk-off angle in the collinear case and the angle between $\mathbf{k}^{\omega,o}$ and $\mathbf{k}^{\omega,e}$ inside the crystal for the non-collinear interaction.

because the saturation phenomenon of type-II CPM is avoided.

(iv) *Effect of temporal walk-off.*

Even if the SHG is phase matched, the fundamental and harmonic group velocities, $v_g(\omega) = \partial\omega/\partial k$, are generally mismatched. This has no effect with continuous wave (c.w.) lasers. For pulsed beams, the temporal separation of the different beams during the propagation can lead to a decrease of the temporal overlap of the pulses. Indeed, this walk-off in the time domain affects the conversion efficiency when the pulse separations are close to the pulse durations. Then after a certain distance, L_τ, the pulses are completely separated, which entails a saturation of the conversion efficiency, for both types I and II (Tomov *et al.*, 1982). Three group velocities must be considered for type II. Type I is simpler, because the two fundamental waves have the same velocity, so $L_\tau = \tau/[v_g^{-1}(\omega) - v_g^{-1}(2\omega)]$, which defines the optimum crystal length, where τ is the pulse duration. For type-I SHG of 532 nm in KH_2PO_4 (KDP), $v_g(266\text{ nm}) = 1.84 \times 10^8\text{ m s}^{-1}$ and $v_g(532\text{ nm}) = 1.94 \times 10^8\text{ m s}^{-1}$, so $L_\tau = 3.5$ mm for 1 ps. For the usual nonlinear crystals, the temporal walk-off must be taken into account for pico- and femtosecond pulses.

1.7.3.3.2.2. *Non-resonant SHG with undepleted pump and transverse and longitudinal Gaussian beams*

We now consider the general situation where the crystal length can be larger than the Rayleigh length.

The Gaussian electric field amplitudes of the two eigen electric field vectors inside the nonlinear crystal are given by

$$E^{\pm}(X, Y, Z) = E_o^{\pm}\frac{w_o}{w(Z)}\exp\left[-\frac{(X+\rho^+Z)^2+(Y+\rho^-Z)^2}{w^2(Z)}\right] \times \exp\left(i\left\{k^{\pm}Z - \arctan(Z/z_R) + \frac{k^{\pm}\left[(X+\rho^+Z)^2+(Y+\rho^-Z)^2\right]}{2Z\left[1+(z_R^2/Z^2)\right]}\right\}\right) \quad (1.7.3.55)$$

with $\rho^- = 0$ for E^+ and $\rho^+ = 0$ for E^-.

(X, Y, Z) is the wave frame defined in Fig. 1.7.3.1. $E_o^{\pm}$ is the scalar complex amplitude at $(X, Y, Z) = (0, 0, 0)$ in the vibration planes $\Pi^{\pm}$.

We consider the refracted waves E^+ and E^- to have the same longitudinal profile inside the crystal. Then the $(1/e^2)$ beam radius is given by $w(Z)^2 = w_o^2[1 + (Z^2/z_R^2)]$, where w_o is the minimum beam radius located at $Z = 0$ and $z_R = kw_o^2/2$, with $k = (k^+ + k^-)/2$; z_R is the Rayleigh length, the length over which the beam radius remains essentially collimated; $k^{\pm}$ are the wavevectors at the wavelength λ in the direction of propagation Z. The far-field half divergence angle is $\Delta\alpha = 2/kw_o$.

The coordinate systems of (1.7.3.22) are identical to those of the parallel-beam limit defined in (iii).

In these conditions and by assuming the undepleted pump approximation, the integration of (1.7.3.22) over (X, Y, Z) leads to the following expression of the power conversion efficiency (Zondy, 1991):

$$\eta_{\text{SHG}}(L) = \frac{P^{2\omega}(L)}{P^{\omega}(0)} = CLP^{\omega}(0)\frac{h(L, w_o, \rho, f, \Delta k)}{\cos^2\rho_{2\omega}}$$

with

$$C = 5.95 \times 10^{-2}\frac{2N-1}{N}\frac{d_{\text{eff}}^2}{\lambda_\omega^3}\frac{n_1^\omega + n_2^\omega}{2}\frac{T_3^{2\omega}T_1^\omega T_2^\omega}{n_3^{2\omega}n_1^\omega n_2^\omega} \quad (\text{W}^{-1}\text{ m}^{-1}) \quad (1.7.3.56)$$

in the same units as equation (1.7.3.42).

For type I, $n_1^\omega = n_2^\omega$, $T_1^\omega = T_2^\omega$, and for type II $n_1^\omega \neq n_2^\omega$, $T_1^\omega \neq T_2^\omega$.

The attenuation coefficient is written

$$h(L, w_o, \rho, f, \Delta k) = [2z_R(\pi)^{1/2}/L]\int_{-\infty}^{+\infty}|H(a)|^2\exp(-4a^2)\,\mathrm{d}a$$

with

$$H(a) = \frac{1}{(2\pi)^{1/2}}\int_{-fL/z_R}^{L(1-f)/z_R}\frac{\mathrm{d}\tau}{1+i\tau}\exp\left[-\gamma^2\left(\tau + \frac{fL}{z_R}\right)^2 - i\sigma\tau\right]$$

$$\text{for type I: } \gamma = 0 \text{ and } \sigma = \Delta k z_R + 4\frac{\rho z_R}{w_o}a$$

$$\text{for type II: } \gamma = \frac{\rho z_R}{w_o(2)^{1/2}} \text{ and } \sigma = \Delta k z_R + 2\frac{\rho z_R}{w_o}a, \quad (1.7.3.57)$$

where f gives the position of the beam waist inside the crystal: $f = 0$ at the entrance and $f = 1$ at the exit surface. The definition and approximations relative to ρ are the same as those discussed for the parallel-beam limit. Δk is the mismatch parameter, which takes into account first a possible shift of the pump beam direction from the collinear phase-matching direction and secondly the distribution of mismatch, including collinear and non-collinear interactions, due to the divergence of the beam, even if the beam axis is phase-matched.

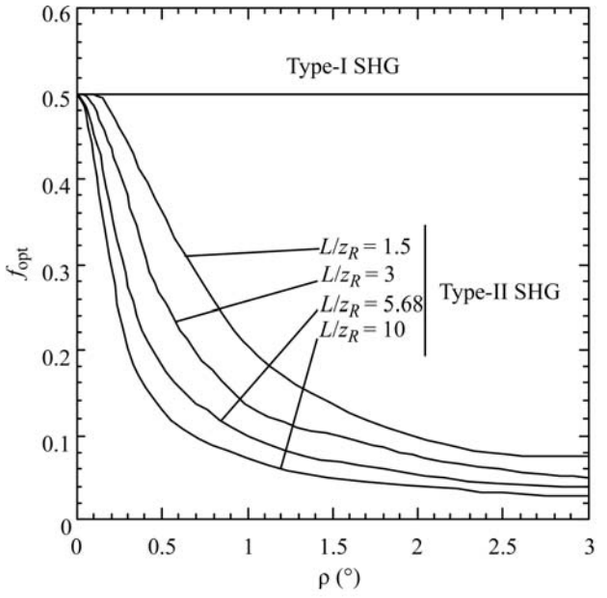

Fig. 1.7.3.12. Position f_{opt} of the beam waist for different values of walk-off angles and L/z_R, leading to an optimum SHG conversion efficiency. The value $f_{opt} = 0.5$ corresponds to the middle of the crystal and $f_{opt} = 0$ corresponds to the entrance surface (Fève & Zondy, 1996).

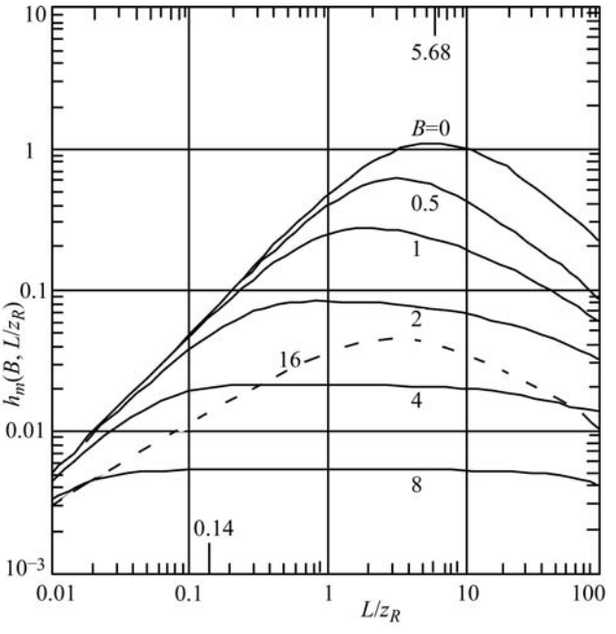

Fig. 1.7.3.13. Optimum walk-off function $h_m(B, L)$ as a function of L/z_R for various values of $B = (1/2)\rho\{[(k_o^\omega + k_e^\omega)/2]L\}^{1/2}$. The curve at $B = 0$ is the same for both type-I and type-II phase matching. The full lines at $B \neq 0$ are for type II and the dashed line at $B = 16$ is for type I. (From Zondy, 1990).

The computation of $h(L, w_o, \rho, f, \Delta k)$ allows an optimization of the SHG conversion efficiency which takes into account L/z_R, the waist location f inside the crystal and the phase mismatch Δk.

Fig. 1.7.3.12 shows the calculated waist location which allows an optimal SHG conversion efficiency for types I and II with optimum phase matching. From Fig. 1.7.3.12, it appears that the optimum waist location for type I, which leads to an optimum conversion efficiency, is exactly at the centre of the crystal, $f_{opt} = 0.5$. For type II, the focusing (L/z_R) is stronger and the walk-off angle is larger, and the optimum waist location is nearer the entrance of the crystal. These facts can be physically understood: for type I, there is no walk-off for the fundamental beam, so the whole crystal length is efficient and the symmetrical configuration is obviously the best one; for type II, the two fundamental rays can be completely separated in the waist area, which has the strongest intensity, when the waist location is far from the entrance face; for a waist location nearer the entrance, the waist area can be selected and the enlargement of the beams from this area allows a spatial overlap up to the exit face, which leads to a higher conversion efficiency.

The divergence of the pump beam imposes non-collinear interactions such that it could be necessary to shift the direction of propagation of the beam from the collinear phase-matching direction in order to optimize the conversion efficiency. This leads to the definition of an optimum phase-mismatch parameter Δk_{opt} $(\neq 0)$ for a given L/z_R and a fixed position of the beam waist f inside the crystal.

The function $h(L, w_o, \rho, f_{opt}, \Delta k_{opt})$, written $h_m(B, L)$, is plotted in Fig. 1.7.3.13 as a function of L/z_R for different values of the walk-off parameter, defined as $B = (1/2)\rho\{[(k_o^\omega + k_e^\omega)/2]L\}^{1/2}$, at the optimal waist location and phase mismatch.

Consider first the case of angular NCPM $(B = 0)$ where type-I and -II conversion efficiencies obviously have the same L/z_R evolutions. An optimum focusing at $L/z_R = 5.68$ exists which defines the optimum focusing $z_{R_{opt}}$ for a given crystal length or the optimal length L_{opt} for a given focusing. The conversion efficiency decreases for $L/z_R > 5.68$ because the increase of the 'average' beam radius over the crystal length due to the strong focusing becomes more significant than the increased peak power in the waist area.

In the case of angular CPM $(B \neq 0)$, the L/z_R variation of type-I conversion efficiency is different from that of type II. For type I, as B increases, the efficiency curves keep the same shape, with their maxima abscissa shifting from $L/z_R = 5.68$ $(B = 0)$ to 2.98 $(B = 16)$ as the corresponding amplitudes decrease. For type II, an optimum focusing becomes less and less appearent, while $(L/z_R)_{opt}$ shifts to much smaller values than for type I for the same variation of B; the decrease of the maximum amplitude is stronger in the case of type II. The calculation of the conversion efficiency as a function of the crystal length L at a fixed z_R shows a saturation for type II, in contrast to type I. The saturation occurs at $B \simeq 3$ with a corresponding focusing parameter $L/z_R \simeq 0.4$, which is the limit of validity of the parallel-beam approximation. These results show that weak focusing is suitable for type II, whereas type I allows higher focusing.

The curves of Fig. 1.7.3.14 give a clear illustration of the walk-off effect in several usual situations of crystal length, walk-off angle and Gaussian laser beam. The SHG conversion efficiency is calculated from formula (1.7.3.56) and from the function (1.7.3.57) at f_{opt} and Δk_{opt}.

1.7.3.3.2.3. *Non-resonant SHG with depleted pump in the parallel-beam limit*

The analytical integration of the three coupled equations (1.7.3.22) with depletion of the pump and phase mismatch has only been done in the parallel-beam limit and by neglecting the walk-off effect (Armstrong *et al.*, 1962; Eckardt & Reintjes, 1984; Eimerl, 1987; Milton, 1992). In this case, the three coordinate systems of equations (1.7.3.22) are identical, (X, Y, Z), and the general solution may be written in terms of the Jacobian elliptic function $\mathrm{sn}(m, \alpha)$.

For the simple case of type I, *i.e.* $E_1^\omega(X, Y, Z) = E_2^\omega(X, Y, Z) = E^\omega(X, Y, Z) = E_{tot}^\omega(X, Y, Z)/(2^{1/2})$, the exit second harmonic intensity generated over a length L is given by (Eckardt & Reintjes, 1984)

$$I^{2\omega}(X, Y, L) = I_{tot}^\omega(X, Y, 0) T^{2\omega} T^\omega v_b^2 \mathrm{sn}^2\left[\frac{\Gamma(X, Y)L}{v_b}, v_b^4\right]. \quad (1.7.3.58)$$

$I^{\omega}_{\rm tot}(X, Y, 0) = 2I^{\omega}(X, Y, 0)$ is the total initial fundamental intensity, $T^{2\omega}$ and T^{ω} are the transmission coefficients,

$$\frac{1}{v_b} = \frac{\Delta s}{4} + \left[1 + \left(\frac{\Delta s}{4}\right)^2\right]^{1/2}$$

with

$$\Delta s = (k^{2\omega} - k^{\omega})/\Gamma$$

and

$$\Gamma(X, Y) = \frac{\omega d_{\rm eff}}{cn^{2\omega}}(T^{\omega})^{1/2}|E^{\omega}_{\rm tot}(X, Y, 0)|. \qquad (1.7.3.59)$$

For the case of phase matching ($k^{\omega} = k^{2\omega}$, $T^{\omega} = T^{2\omega}$), we have $\Delta s = 0$ and $v_b = 1$, and the Jacobian elliptic function sn$(m, 1)$ is equal to tanh(m). Then formula (1.7.3.58) becomes

$$I^{2\omega}(X, Y, L) = I^{\omega}_{\rm tot}(X, Y, 0)(T^{\omega})^2 \tanh^2[\Gamma(X, Y)L], \qquad (1.7.3.60)$$

where $\Gamma(X, Y)$ is given by (1.7.3.59).

The exit fundamental intensity $I^{\omega}(X, Y, L)$ can be established easily from the harmonic intensity (1.7.3.60) according to the Manley–Rowe relations (1.7.2.40), *i.e.*

$$I^{\omega}(X, Y, L) = I^{\omega}_{\rm tot}(X, Y, 0)(T^{\omega})^2 {\rm sech}^2[\Gamma(X, Y)L]. \qquad (1.7.3.61)$$

For small ΓL, the functions $\tanh^2(\Gamma L) \simeq \Gamma^2 L^2$ and ${\rm sn}^2[(\Gamma L/v_b), v_b^4] \simeq \sin^2(\Gamma L/v_b)$ with $v_b \simeq 2/\Delta s$.

The first consequence of formulae (1.7.3.58)–(1.7.3.59) is that the various acceptance bandwidths decrease with increasing ΓL. This fact is important in relation to all the acceptances but in particular for the thermal and angular ones. Indeed, high efficiencies are often reached with high power, which can lead to an important heating due to absorption. Furthermore, the divergence of the beams, even small, creates a significant dephasing: in this case, and even for a propagation along a phase-matching direction, formula (1.7.3.60) is not valid and may be replaced by (1.7.3.58) where $k(2\omega) - k(\omega)$ is considered as the 'average' mismatch of a parallel beam.

In fact, there always exists a residual mismatch due to the divergence of real beams, even if not focused, which forbids asymptotically reaching a 100% conversion efficiency: $I^{2\omega}(L)$ increases as a function of ΓL until a maximum value has been reached and then decreases; $I^{2\omega}(L)$ will continue to rise and fall as ΓL is increased because of the periodic nature of the Jacobian elliptic sine function. Thus the maximum of the conversion efficiency is reached for a particular value $(\Gamma L)_{\rm opt}$. The determination of $(\Gamma L)_{\rm opt}$ by numerical computation allows us to define the optimum incident fundamental intensity $I^{\omega}_{\rm opt}$ for a given phase-matching direction, characterized by K, and a given crystal length L.

The crystal length must be optimized in order to work with an incident intensity $I^{\omega}_{\rm opt}$ smaller than the damage threshold intensity $I^{\omega}_{\rm dam}$ of the nonlinear crystal, given in Section 1.7.5 for the main materials.

Formula (1.7.3.57) is established for type I. For type II, the second harmonic intensity is also an sn^2 function where the

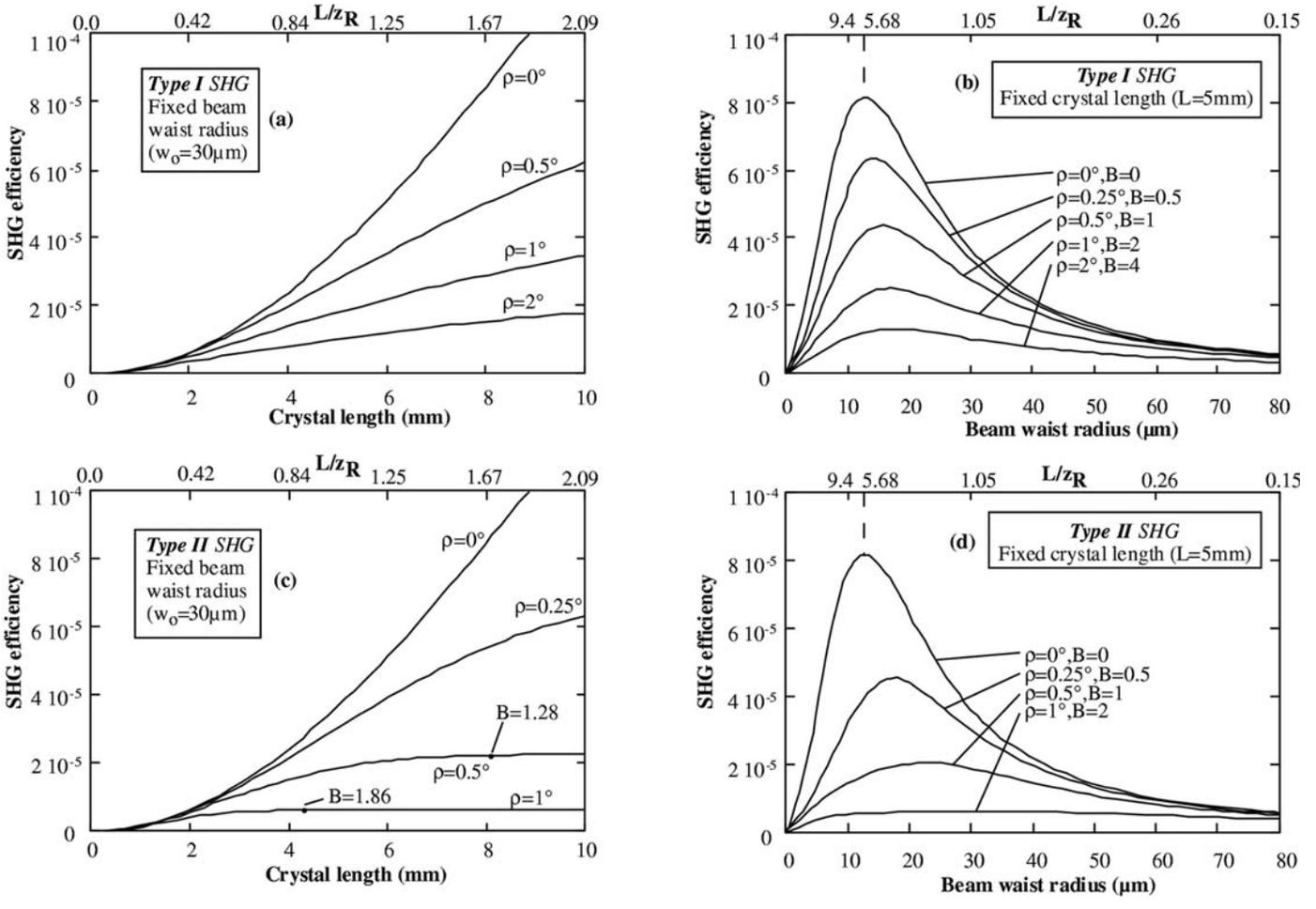

Fig. 1.7.3.14. Type-I and -II conversion efficiencies calculated as a function of L/z_R for different typical walk-off angles ρ: (*a*) and (*c*) correspond to a fixed focusing condition (w_o = 30 μm); the curves (*b*) and (*d*) are plotted for a constant crystal length (L = 5 mm); all the calculations are performed with the same effective coefficient ($d_{\rm eff}$ = 1 pm V^{-1}), refractive indices ($n_3^{2\omega}n_1^{\omega}n_2^{\omega} = 5.83$) and fundamental power [$P_{\omega}(0 = 1$ W]. B is the walk-off parameter defined in the text (Fève & Zondy, 1996).

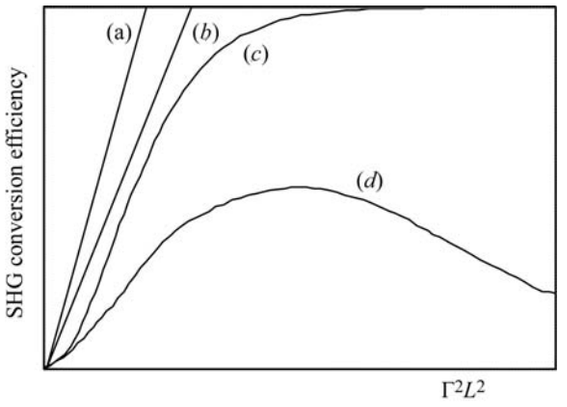

Fig. 1.7.3.15. Schematic SHG conversion efficiency for different situations of pump depletion and dephasing. (*a*) No depletion, no dephasing, $\eta = \Gamma^2L^2$; (*b*) no depletion with constant dephasing δ, $\eta = \Gamma^2L^2 \sin c^2\delta$; (*c*) depletion without dephasing, $\eta = \tanh^2(\Gamma L)$; (*d*) depletion and dephasing, $\eta = \eta_m \mathrm{sn}^2(\Gamma L/v_b, v_b^4)$.

intensities of the two fundamental beams $I_1^\omega(X, Y, 0)$ and $I_2^\omega(X, Y, 0)$, which are not necessarily equal, are taken into account (Eimerl, 1987): the $\tanh^2$ function is valid only if perfect phase matching is achieved and if $I_1^\omega(X, Y, 0) = I_2^\omega(X, Y, 0)$, these conditions being never satisfied in real cases.

The situations described above are summarized in Fig. 1.7.3.15.

We give the example of type-II SHG experiments performed with a 10 Hz injection-seeded single-longitudinal-mode ($N = 1$) 1064 nm Nd:YAG (Spectra-Physics DCR-2A-10) laser equipped with super Gaussian mirrors; the pulse is 10 ns in duration and is near a Gaussian single-transverse mode, the beam radius is 4 mm, non-focused and polarized at $\pi/4$ to the principal axes of a 10 mm long KTP crystal ($L\delta\theta$ = 15 mrad cm, $L\delta\varphi$ = 100 mrad cm). The fundamental energy increases from 78 mJ (62 MW cm^{-2}) to 590 mJ (470 MW cm^{-2}), which correponds to the damage of the exit surface of the crystal; for each experiment, the crystal was rotated in order to obtain the maximum conversion efficiency. The peak power SHG conversion efficiency is estimated from the measured energy conversion efficiency multiplied by the ratio between the fundamental and harmonic pulse duration ($\tau_\omega/\tau_{2\omega} = 2^{1/2}$). It increases from 50% at 63 MW cm^{-2} to a maximum value of 85% at 200 MW cm^{-2} and decreases for higher intensities, reaching 50% at 470 MW cm^{-2} (Boulanger, Fejer *et al.*, 1994).

The integration of the intensity profiles (1.7.3.58) and (1.7.3.60) is obvious in the case of incident fundamental beams with a flat energy distribution (1.7.3.36). In this case, the fundamental and harmonic beams inside the crystal have the same profile and radius as the incident beam. Thus the powers are obtained from formulae (1.7.3.58) and (1.7.3.60) by expressing the intensity and electric field modulus as a function of the power, which is given by (1.7.3.38) with $m = 1$.

For a Gaussian incident fundamental beam, (1.7.3.37), the fundamental and harmonic beams are not Gaussian (Eckardt & Reintjes, 1984; Pliszka & Banerjee, 1993).

All the previous intensities are the peak values in the case of pulsed beams. The relation between average and peak powers, and then SHG efficiencies, is much more complicated than the ratio $\tau^{2\omega}/\tau^\omega$ of the undepleted case.

1.7.3.3.2.4. *Resonant SHG*

When the single-pass conversion efficiency SHG is too low, with c.w. lasers for example, it is possible to put the nonlinear crystal in a Fabry–Perot cavity external to the pump laser or directly inside the pump laser cavity, as shown in Figs. 1.7.3.6(*b*) and (*c*). The second solution, described later, is generally used because the available internal pump intensity is much larger.

We first recall some basic and simplified results of laser cavity theory without a nonlinear medium. We consider a laser in which one mirror is 100% reflecting and the second has a transmission T at the laser pulsation ω. The power within the cavity, $P_{\mathrm{in}}(\omega)$, is evaluated at the steady state by setting the round-trip saturated gain of the laser equal to the sum of all the losses. The output laser cavity, $P_{\mathrm{out}}(\omega)$, is given by (Siegman, 1986)

$$P_{\mathrm{out}}(\omega) = TP_{\mathrm{in}}(\omega)$$

with

$$P_{\mathrm{in}}(\omega) = \frac{2g_oL' - (\gamma + T)}{2S(T + \gamma)}. \qquad (1.7.3.62)$$

L' is the laser medium length, $g_o = \sigma N_o$ is the small-signal gain coefficient per unit length of laser medium, σ is the stimulated-emission cross section, N_o is the population inversion without oscillation, S is a saturation parameter characteristic of the nonlinearity of the laser transition, and $\gamma = \gamma_L = 2\alpha_L L' + \beta$ is the loss coefficient where α_L is the laser material absorption coefficient per unit length and β is another loss coefficient including absorption in the mirrors and scattering in both the laser medium and mirrors. For given g_o, S, α_L, β and L', the output power reaches a maximum value for an optimal transmission coefficient T_{opt} defined by $[\partial P_{\mathrm{out}}(\omega)/\partial T]_{T_{\mathrm{opt}}} = 0$, which gives

$$T_{\mathrm{opt}} = (2g_oL'\gamma)^{1/2} - \gamma. \qquad (1.7.3.63)$$

The maximum output power is then given by

$$P_{\mathrm{out}}^{\max}(\omega) = (1/2S)[(2g_oL')^{1/2} - \gamma^{1/2}]^2. \qquad (1.7.3.64)$$

In an intracavity SHG device, the two cavity mirrors are 100% reflecting at ω but one mirror is perfectly transmitting at 2ω. The presence of the nonlinear medium inside the cavity then leads to losses at ω equal to the round-trip-generated second harmonic (SH) power: half of the SH produced flows in the forward direction and half in the backward direction. Hence the highly transmitting mirror at 2ω is equivalent to a nonlinear transmission coefficient at ω which is equal to twice the single-pass SHG conversion efficiency η_{SHG}.

The fundamental power inside the cavity $P_{\mathrm{in}}(\omega)$ is given at the steady state by setting, for a round trip, the saturated gain equal to the sum of the linear and nonlinear losses. $P_{\mathrm{in}}(\omega)$ is then given by (1.7.3.62), where T and γ are (Geusic *et al.*, 1968; Smith, 1970)

$$T = 2\eta_{\mathrm{SHG}} = [P_{\mathrm{out}}(2\omega)/P_{\mathrm{in}}(\omega)] \qquad (1.7.3.65)$$

and

$$\gamma = \gamma_L + \gamma_{NL}. \qquad (1.7.3.66)$$

η_{SHG} is the single-pass conversion efficiency. γ_L and γ_{NL} are the loss coefficients at ω of the laser medium and of the nonlinear crystal, respectively. L is the nonlinear medium length. The two faces of the nonlinear crystal are assumed to be antireflection-coated at ω.

In the undepleted pump approximation, the backward and forward power generated outside the nonlinear crystal at 2ω is

$$P_{\mathrm{out}}(2\omega) = 2KP_{\mathrm{in}}^2(\omega) \qquad (1.7.3.67)$$

with

$$K = B(L^2/w_o^2)\sin c^2(\Delta kL/2),$$

where

$$B = \frac{32\pi}{\varepsilon_o c}\frac{2N-1}{N}\frac{d_{\mathrm{eff}}^2}{\lambda_\omega^2}\frac{T_3^{2\omega}T_1^\omega T_2^\omega}{n_3^{2\omega}n_1^\omega n_2^\omega} \quad (\mathrm{W}^{-1}).$$

The intracavity SHG conversion efficiency is usually defined as the ratio of the SH output power to the maximum output power that would be obtained from the laser without the nonlinear crystal by optimal linear output coupling.

Maximizing (1.7.3.67) with respect to K according to (1.7.3.62), (1.7.3.65) and (1.7.3.66) gives (Perkins & Fahlen, 1987)

$$K_{\rm opt} = (\gamma_L + \gamma_{NL})S \qquad (1.7.3.68)$$

and

$$P_{\rm out}^{\rm max}(2\omega) = (1/2S)[(2g_oL')^{1/2} - (\gamma_L + \gamma_{NL})^{1/2}]^2. \qquad (1.7.3.69)$$

(1.7.3.69) shows that for the case where $\gamma_{\rm NL} \ll \gamma_L$ ($\gamma \simeq \gamma_L$), the maximum SH power is identically equal to the maximum fundamental power, (1.7.3.64), available from the same laser for the same value of loss, which, according to the previous definition of the intracavity efficiency, corresponds to an SHG conversion efficiency of 100%. $P_{\rm out}^{\rm max}(2\omega)$ strongly decreases as the losses $(\gamma_L + \gamma_{\rm NL})$ increase . Thus an efficient intracavity device requires the reduction of all losses at ω and 2ω to an absolute minimum.

(1.7.3.68) indicates that $K_{\rm opt}$ is independent of the operating power level of the laser, in contrast to the optimum transmitting mirror where $T_{\rm opt}$, given by (1.7.3.63), depends on the laser gain. $K_{\rm opt}$ depends only on the total losses and saturation parameter. For given losses, the knowledge of $K_{\rm opt}$ allows us to define the optimal parameters of the nonlinear crystal, in particular the figure of merit, $d_{\rm eff}^2/n_3^{2\omega}n_1^{\omega}n_2^{\omega}$ and the ratio $(L/w_o)^2$, in which the walk-off effect and the damage threshold must also be taken into account.

Some examples: a power of 1.1 W at 0.532 µm was generated in a $\rm TEM_{oo}$ c.w. SHG intracavity device using a 3.4 mm $Ba_2NaNb_5O_{15}$ crystal within a 1.064 µm Nd:YAG laser cavity (Geusic *et al.*, 1968). A power of 9.0 W has been generated at 0.532 µm using a more complicated geometry based on an Nd:YAG intracavity-lens folded-arm cavity configuration using KTP (Perkins & Fahlen, 1987). High-average-power SHG has also been demonstrated with output powers greater than 100 W at 0.532 µm in a KTP crystal inside the cavity of a diode side-pumped Nd:YAG laser (LeGarrec *et al.*, 1996).

For type-II phase matching, a rotated quarter waveplate is useful in order to reinstate the initial polarization of the fundamental waves after a round trip through the nonlinear crystal, the retardation plate and the mirror (Perkins & Driscoll, 1987).

If the nonlinear crystal surface on the laser medium side has a 100% reflecting coating at 2ω and if the other surface is 100% transmitting at 2ω, it is possible to extract the full SH power in one direction (Smith, 1970). Furthermore, such geometry allows us to avoid losses of the backward SH beam in the laser medium and in other optical components behind.

External-cavity SHG also leads to good results. The resonated wave may be the fundamental or the harmonic one. The corresponding theoretical background is detailed in Ashkin *et al.* (1966). For example, a bow-tie configuration allowed the generation of 6.5 W of $\rm TEM_{oo}$ c.w. 0.532 µm radiation in a 6 mm LiB_3O_5 (LBO) crystal; the Nd:YAG laser was an 18 W c.w. laser with an injection-locked single frequency (Yang *et al.*, 1991).

1.7.3.3.3. *Third harmonic generation (THG)*

Fig. 1.7.3.16 shows the three possible ways of achieving THG: a cascading interaction involving two $\chi^{(2)}$ processes, *i.e.* $\omega + \omega = 2\omega$ and $\omega + 2\omega = 3\omega$, in two crystals or in the same crystal, and direct THG, which involves $\chi^{(3)}$, *i.e.* $\omega + \omega + \omega = 3\omega$.

1.7.3.3.3.1. *SHG ($\omega + \omega = 2\omega$) and SFG ($\omega + 2\omega = 3\omega$) in different crystals*

We consider the case of the situation in which the SHG is phase-matched with or without pump depletion and in which the sum-frequency generation (SFG) process ($\omega + 2\omega = 3\omega$), phase-matched or not, is without pump depletion at ω and 2ω. All the waves are assumed to have a flat distribution given by (1.7.3.36) and the walk-off angles are nil, in order to simplify the calculations.

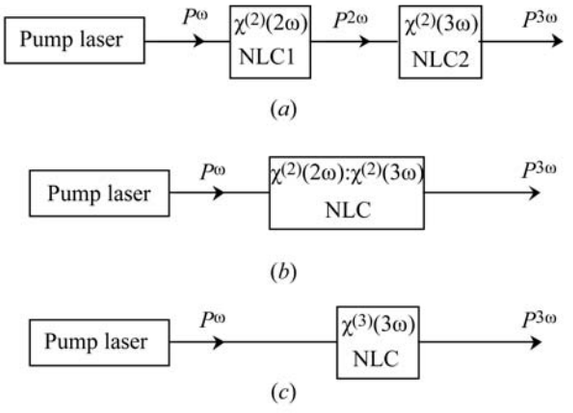

Fig. 1.7.3.16. Configurations for third harmonic generation. (*a*) Cascading process SHG ($\omega + \omega = 2\omega$): SFG ($\omega + 2\omega = 3\omega$) in two crystals NLC1 and NLC2 and (*b*) in a single nonlinear crystal NLC; (*c*) direct process THG ($\omega + \omega + \omega = 3\omega$) in a single nonlinear crystal NLC.

This configuration is the most frequently occurring case because it is unusual to get simultaneous phase matching of the two processes in a single crystal. The integration of equations (1.7.3.22) over Z for the SFG in the undepleted pump approximation with $E_1^{\omega}(Z_{\rm SFG} = 0) = E_1^{\omega}(L_{\rm SHG})$, $E_2^{2\omega}(Z_{\rm SFG} = 0) = E_2^{2\omega}(L_{\rm SHG})$ and $E_3^{3\omega}(Z_{\rm SFG} = 0) = 0$, followed by the integration over the cross section leads to

$$P^{3\omega}(L_{\rm SFG}) = B_{\rm SFG}[aP^{\omega}(L_{\rm SHG})]P^{2\omega}(L_{\rm SHG})\frac{L_{\rm SFG}^2}{w_o^2}\sin c^2\frac{\Delta k_{\rm SFG}L_{\rm SFG}}{2} \quad ({\rm W})$$

with

$$B_{\rm SFG} = \frac{72\pi}{\varepsilon_o c}\frac{2N-1}{N}\frac{d_{\rm eff}^2}{\lambda_{\omega}^2}\frac{T_3^{3\omega}T_1^{\omega}T_2^{2\omega}}{n_3^{3\omega}n_1^{\omega}n_2^{2\omega}} \quad ({\rm W}^{-1})$$

$$a = 1 \text{ for type-I SHG}, \quad a = \tfrac{1}{2} \text{ for type-II SHG}. \qquad (1.7.3.70)$$

$P^{\omega}(L_{\rm SHG})$ and $P^{2\omega}(L_{\rm SHG})$ are the fundamental and harmonic powers, respectively, at the exit of the first crystal. $L_{\rm SHG}$ and $L_{\rm SFG}$ are the lengths of the first and the second crystal, respectively. $\Delta k_{\rm SFG} = k^{3\omega} - (k^{\omega} + k^{2\omega})$ is the SFG phase mismatch. λ_{ω} is the fundamental wavelength. The units and other parameters are as defined in (1.7.3.42).

For type-II SHG, the fundamental waves are polarized in two orthogonal vibration planes, so only half of the fundamental power can be used for type-I, -II or -III SFG ($a = 1/2$), in contrast to type-I SHG ($a = 1$). In the latter case, and for type-I SFG, it is necessary to set the fundamental and second harmonic polarizations parallel.

The cascading conversion efficiency is calculated according to (1.7.3.61) and (1.7.3.70); the case of type-I SHG gives, for example,

$$\eta_{\rm THG}(L_{\rm SHG}, L_{\rm SFG}) = \frac{P^{3\omega}(L_{\rm SFG})}{P_{\rm tot}^{\omega}(0)} = B_{\rm SFG}(T^{\omega})^4P_{\rm tot}^{\omega}(0)\tanh^2(\Gamma L_{\rm SHG}) \times \operatorname{sech}^2(\Gamma L_{\rm SHG})\frac{L_{\rm SFG}^2}{w_o^2}\sin c^2\left(\frac{\Delta k_{\rm SFG}L_{\rm SFG}}{2}\right), \qquad (1.7.3.71)$$

where Γ is as in (1.7.3.59).

(n^{ω}, T^{ω}) are relative to the phase-matched SHG crystal and $(n_1^{\omega}, n_2^{2\omega}, n_3^{3\omega}, T_1^{\omega}, T_2^{2\omega}, T_3^{3\omega})$ correspond to the SFG crystal.

In the undepleted pump approximation for SHG, (1.7.3.71) becomes (Qiu & Penzkofer, 1988)

$$\eta_{\mathrm{THG}}(L_{\mathrm{SHG}}, L_{\mathrm{SFG}}) = BT^{\omega}\left[\frac{P^{\omega}(0)}{w_o^2}\right]^2 L_{\mathrm{SHG}}^2 L_{\mathrm{SFG}}^2 \sin c^2\left(\frac{\Delta k_{\mathrm{SFG}} L_{\mathrm{SFG}}}{2}\right) \tag{1.7.3.72}$$

with

$$B = B_{\mathrm{SHG}} \cdot B_{\mathrm{SFG}} = \frac{576\pi^2}{\varepsilon_o^2 c^2}\left(\frac{2N-1}{N}\right)^2 \frac{d_{\mathrm{eff_{SHG}}}^2 d_{\mathrm{eff_{SFG}}}^2}{\lambda_{\omega}^4}\left(\frac{T_{\mathrm{SHG}}^3}{n_{\mathrm{SHG}}^3}\right)\left(\frac{T_{\mathrm{SFG}}^3}{n_{\mathrm{SFG}}^3}\right)$$

in W^{-2}, where

$$\frac{T_{\mathrm{SHG}}^3}{n_{\mathrm{SHG}}^3} = \frac{(T^{\omega})^3}{(n^{\omega})^3} \quad \text{and} \quad \frac{T_{\mathrm{SFG}}^3}{n_{\mathrm{SFG}}^3} = \frac{T_3^{3\omega} T_1^{\omega} T_2^{2\omega}}{n_3^{3\omega} n_1^{\omega} n_2^{2\omega}}.$$

The units are the same as in (1.7.3.42).

A more general case of SFG, where one of the two pump beams is depleted, is given in Section 1.7.3.3.4.

1.7.3.3.3.2. *SHG ($\omega + \omega = 2\omega$) and SFG ($\omega + 2\omega = 3\omega$) in the same crystal*

When the SFG conversion efficiency is sufficiently low in comparison with that of the SHG, it is possible to integrate the equations relative to SHG and those relative to SFG separately (Boulanger, Fejer *et al.*, 1994). In order to compare this situation with the example taken for the previous case, we consider a type-I configuration of polarization for SHG. By assuming a perfect phase matching for SHG, the amplitude of the third harmonic field inside the crystal is (Boulanger, 1994)

$$E^{3\omega}(X, Y, Z) = jK^{3\omega}(\varepsilon_o \chi_{\mathrm{eff_{SFG}}}) \times \int_0^L E_{\mathrm{tot}}^{\omega}(X, Y, Z) E^{2\omega}(X, Y, Z) \exp(j\Delta k_{\mathrm{SFG}} Z)\, \mathrm{d}Z \tag{1.7.3.73}$$

with

$$E^{2\omega}(X, Y, Z) = (T^{\omega})^{1/2} |E_{\mathrm{tot}}^{\omega}(0)| \tanh(\Gamma Z)$$
$$\text{and} \quad E_{\mathrm{tot}}^{\omega}(X, Y, Z) = (T^{\omega})^{1/2} |E_{\mathrm{tot}}^{\omega}(0)| \operatorname{sech}(\Gamma Z). \tag{1.7.3.74}$$

Γ is as in (1.7.3.59).

(1.7.3.73) can be analytically integrated for undepleted pump SHG; $\operatorname{sech}(m) \to 1$, $\tanh(m) \to m$, and so we have

$$\eta_{\mathrm{THG}}(L) = P^{3\omega}(L)/P_{\mathrm{tot}}^{\omega}(0) \tag{1.7.3.75}$$

with

$$P^{3\omega}(L) = \frac{576\pi^2}{\varepsilon_o^2 c^2}\left(\frac{2N-1}{N}\right)^2 T^{3\omega} \frac{d_{\mathrm{eff_{SHG}}}^2 d_{\mathrm{eff_{SFG}}}^2}{n^{3\omega}(n^{\omega})^3 (n^{2\omega})^2} \frac{[T^{\omega} P_{\mathrm{tot}}^{\omega}(0)]^3}{w_o^4 \lambda_{\omega}^4} J(L),$$

where the integral $J(L)$ is

$$J(L) = \left| \int_0^L Z \exp(i\Delta k_{\mathrm{SFG}} Z)\, \mathrm{d}Z \right|^2. \tag{1.7.3.76}$$

For a nonzero SFG phase mismatch, $\Delta k_{\mathrm{SFG}} \neq 0$,

$$J(L) \simeq L^2/(\Delta k_{\mathrm{SFG}})^2. \tag{1.7.3.77}$$

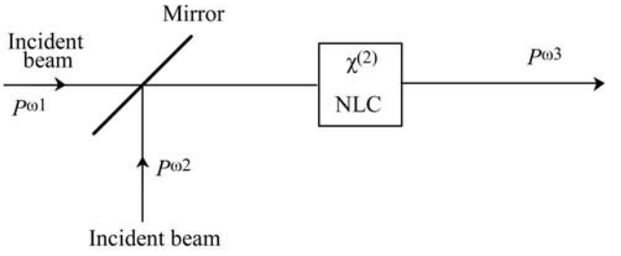

Fig. 1.7.3.17. Frequency up-conversion process $\omega_1 + \omega_2 = \omega_3$. The beam at ω_1 is mixed with the beam at ω_2 in the nonlinear crystal NLC in order to generate a beam at ω_3. $P^{\omega_1,\omega_2,\omega_3}$ are the different powers.

For phase-matched SFG, $\Delta k_{\mathrm{SFG}} = 0$,

$$J(L) = L^4/4. \tag{1.7.3.78}$$

Therefore (1.7.3.75) according to (1.7.3.78) is equal to (1.7.3.72) with $L_{\mathrm{SHG}} = L_{\mathrm{SFG}} = L/2$, $\Delta k_{\mathrm{SFG}} = 0$ and 100% transmission coefficients at ω and 2ω between the two crystals.

1.7.3.3.3.3. *Direct THG ($\omega + \omega + \omega = 3\omega$)*

As for the cascading process, we consider a flat plane wave which propagates in a direction without walk-off. The integration of equations (1.7.3.24) over the crystal length L, with $E_4^{3\omega}(X, Y, 0) = 0$ and in the undepleted pump approximation, leads to

$$E_4^{3\omega}(X, Y, L) = jK_4^{3\omega}[\varepsilon_o \chi_{\mathrm{eff}}^{(3)}] E_1^{\omega}(X, Y, 0) E_2^{\omega}(X, Y, 0) E_3^{\omega}(X, Y, 0) \times L \sin c[(\Delta k \cdot L)/2] \exp(-j\Delta k L/2). \tag{1.7.3.79}$$

According to (1.7.3.36) and (1.7.3.38), the integration of (1.7.3.79) over the cross section, which is the same for the four beams, leads to

$$\eta_{\mathrm{THG}}(L) = \frac{P^{3\omega}(L)}{P^{\omega}(0)} = B_{\mathrm{THG}}[P^{\omega}(0)]^2 \frac{L^2}{w_o^4} \sin c^2[(\Delta k \cdot L)/2]$$

with

$$B_{\mathrm{THG}} = \frac{576}{\varepsilon_o^2 c^2} \frac{d_{\mathrm{eff}}^2}{\lambda_{\omega}^2} \frac{T_4^{3\omega} (T_1^{\omega})^2 T_2^{\omega}}{n_4^{3\omega} (n_1^{\omega})^2 n_2^{\omega}} \quad (\mathrm{m^2\ W^{-2}}), \tag{1.7.3.80}$$

where $d_{\mathrm{eff}} = (1/4)\chi_{\mathrm{eff}}^{(3)}$ is in $\mathrm{m^2\ V^{-2}}$ and λ_{ω} is in m. The statistical factor is assumed to be equal to 1, which corresponds to a longitudinal single-mode laser.

The different types of phase matching and the associated relations and configurations of polarization are given in Table 1.7.3.2 by considering the SFG case with $\omega_1 = \omega_2 = \omega_3 = \omega_4/3$.

1.7.3.3.4. *Sum-frequency generation (SFG)*

SHG ($\omega + \omega = 2\omega$) and SFG ($\omega + 2\omega = 3\omega$) are particular cases of three-wave SFG. We consider here the general situation where the two incident beams at ω_1 and ω_2, with $\omega_1 < \omega_2$, interact with the generated beam at ω_3, with $\omega_3 = \omega_1 + \omega_2$, as shown in Fig. 1.7.3.17. The phase-matching configurations are given in Table 1.7.3.1.

From the general point of view, SFG is a frequency up-conversion parametric process which is used for the conversion of laser beams at low circular frequency: for example, conversion of infrared to visible radiation.

The resolution of system (1.7.3.22) leads to Jacobian elliptic functions if the waves at ω_1 and ω_2 are both depleted. The calculation is simplified in two particular situations which are often encountered: on the one hand undepletion for the waves at ω_1 and ω_2, and on the other hand depletion of only one wave at

ω_1 or ω_2. For the following, we consider plane waves which propagate in a direction without walk-off so we consider a single wave frame; the energy distribution is assumed to be flat, so the three beams have the same radius w_o.

1.7.3.3.4.1. *SFG ($\omega_1 + \omega_2 = \omega_3$) with undepletion at ω_1 and ω_2*

The resolution of system (1.7.3.22) with $E_1(X, Y, 0) \neq 0$, $E_2(X, Y, 0) \neq 0$, $\partial E_1(X, Y, Z)/\partial Z = \partial E_2(X, Y, Z)/\partial Z = 0$ and $E_3(X, Y, 0) = 0$, followed by integration over (X, Y), leads to

$$P^{\omega_1}(L) = (T^{\omega_1})^2 P^{\omega_1}(0) \tag{1.7.3.81}$$

$$P^{\omega_2}(L) = (T^{\omega_2})^2 P^{\omega_2}(0) \tag{1.7.3.82}$$

$$P^{\omega_3}(L) = BP^{\omega_1}(0)P^{\omega_2}(0)\frac{L^2}{w_o^2}\sin c^2\frac{\Delta k \cdot L}{2} \tag{1.7.3.83}$$

with

$$B_{\text{SFG}} = \frac{72\pi}{\varepsilon_o c}\frac{2N-1}{N}\frac{d_{\text{eff}}^2}{\lambda_\omega^2}\frac{T^{\omega_3}T^{\omega_1}T^{\omega_2}}{n^{\omega_3}n^{\omega_1}n^{\omega_2}} \quad (\text{W}^{-1})$$

in the same units as equation (1.7.3.70).

1.7.3.3.4.2. *SFG ($\omega_s + \omega_p = \omega_i$) with undepletion at ω_p*

$(\omega_s, \omega_p, \omega_i) = (\omega_1, \omega_2, \omega_3)$ or $(\omega_2, \omega_1, \omega_3)$.

The undepleted wave at ω_p, the pump, is mixed in the nonlinear crystal with the depleted wave at ω_s, the signal, in order to generate the idler wave at $\omega_i = \omega_s + \omega_p$. The integrations of the coupled amplitude equations over (X, Y, Z) with $E_s(X, Y, 0) \neq 0$, $E_p(X, Y, 0) \neq 0$, $\partial E_p(X, Y, Z)/\partial Z = 0$ and $E_i(X, Y, 0) = 0$ give

$$P_p(L) = T_p^2 P_p(0) \tag{1.7.3.84}$$

$$P_i(L) = \frac{\omega_i}{\omega_s}P_s(0)\Gamma^2L^2\frac{\sin^2\{\Gamma^2L^2 + [(\Delta k \cdot L)/2]^2\}^{1/2}}{\Gamma^2L^2 + [(\Delta k \cdot L)/2]^2} \tag{1.7.3.85}$$

$$P_s(L) = P_s(0)\left[1 - \frac{\omega_s}{\omega_i}\frac{P_i(L)}{P_s(0)}\right], \tag{1.7.3.86}$$

with $\Delta k = k_i - (k_s + k_p)$ and $\Gamma^2 = [B_s P_p(0)]/w_o^2$, where

$$B_s = \frac{8\pi}{\varepsilon_o c}\frac{2N-1}{N}\frac{d_{\text{eff}}^2}{\lambda_s\lambda_i}\frac{T_s T_p T_i}{n_s n_p n_i}.$$

Thus, even if the up-conversion process is phase-matched ($\Delta k = 0$), the power transfers are periodic: the photon transfer efficiency is then 100% for $\Gamma L = (2m+1)(\pi/2)$, where m is an integer, which allows a maximum power gain ω_i/ω_s for the idler. A nonlinear crystal with length $L = (\pi/2\Gamma)$ is sufficient for an optimized device.

For a small conversion efficiency, *i.e.* ΓL weak, (1.7.3.85) and (1.7.3.86) become

$$P_i(L) \simeq P_s(0)\frac{\omega_i}{\omega_s}\Gamma^2L^2\sin c^2\frac{\Delta k \cdot L}{2} \tag{1.7.3.87}$$

and

$$P_s(L) \simeq P_s(0). \tag{1.7.3.88}$$

The expression for $P_i(L)$ with $\Delta k = 0$ is then equivalent to (1.7.3.83) with $\omega_p = \omega_1$ or ω_2, $\omega_i = \omega_3$ and $\omega_s = \omega_2$ or ω_1.

For example, the frequency up-conversion interaction can be of great interest for the detection of a signal, ω_s, comprising IR radiation with a strong divergence and a wide spectral bandwidth. In this case, the achievement of a good conversion efficiency, $P_i(L)/P_s(0)$, requires both wide spectral and angular acceptance bandwidths with respect to the signal. The double non-criticality in frequency and angle (DNPM) can then be used with one-beam non-critical non-collinear phase matching (OBNC) associated with vectorial group phase matching (VGPM) (Dolinchuk *et al.*, 1994): this corresponds to the equality of the absolute magnitudes and directions of the signal and idler group velocity vectors *i.e.* $\mathrm{d}\omega_i/\mathrm{d}\mathbf{k}_i = \mathrm{d}\omega_s/\mathrm{d}\mathbf{k}_s$.

1.7.3.3.5. *Difference-frequency generation (DFG)*

DFG is defined by $\omega_3 - \omega_1 = \omega_2$ with $E_2(X, Y, 0) = 0$ or $\omega_3 - \omega_2 = \omega_1$ with $E_1(X, Y, 0) = 0$. The DFG phase-matching configurations are given in Table 1.7.3.1. As for SFG, the solutions of system (1.7.3.22) are Jacobian elliptic functions when the incident waves are both depleted. We consider here the simplified situations of undepletion of the two incident waves and depletion of only one incident wave. In the latter, the solutions differ according to whether the circular frequency of the undepleted wave is the highest one, *i.e.* ω_3, or not. We consider the case of plane waves that propagate in a direction without walk-off and we assume a flat energy distribution for the three beams.

1.7.3.3.5.1. *DFG ($\omega_p - \omega_s = \omega_i$) with undepletion at ω_p and ω_s*

$(\omega_s, \omega_i, \omega_p) = (\omega_1, \omega_2, \omega_3)$ or $(\omega_2, \omega_1, \omega_3)$.

The resolution of system (1.7.3.22) with $E_s(X, Y, 0) \neq 0$, $E_p(X, Y, 0) \neq 0$, $\partial E_p(X, Y, Z)/\partial Z = \partial E_s(X, Y, Z)/\partial Z = 0$ and $E_i(X, Y, 0) = 0$, followed by integration over (X, Y), leads to the same solutions as for SFG with undepletion at ω_1 and ω_2, *i.e.* formulae (1.7.3.81), (1.7.3.82) and (1.7.3.83), by replacing ω_1 by ω_s, ω_2 by ω_p and ω_3 by ω_i. A schematic device is given in Fig. 1.7.3.17 by replacing $(\omega_1, \omega_2, \omega_3)$ by $(\omega_1, \omega_3, \omega_2)$ or $(\omega_2, \omega_3, \omega_1)$.

1.7.3.3.5.2. *DFG ($\omega_s - \omega_p = \omega_i$) with undepletion at ω_p*

$(\omega_s, \omega_i, \omega_p) = (\omega_3, \omega_1, \omega_2)$ or $(\omega_3, \omega_2, \omega_1)$.

The resolution of system (1.7.3.22) with $E_s(X, Y, 0) \neq 0$, $E_p(X, Y, 0) \neq 0$, $\partial E_p(X, Y, Z)/\partial Z = 0$ and $E_i(X, Y, 0) = 0$, followed by the integration over (X, Y), leads to the same solutions as for SFG with undepletion at ω_1 or ω_2: formulae (1.7.3.84), (1.7.3.85) and (1.7.3.86).

1.7.3.3.5.3. *DFG ($\omega_p - \omega_s = \omega_i$) with undepletion at ω_p – optical parametric amplification (OPA), optical parametric oscillation (OPO)*

$(\omega_s, \omega_i, \omega_p) = (\omega_1, \omega_2, \omega_3)$ or $(\omega_2, \omega_1, \omega_3)$.

The initial conditions are the same as in Section 1.7.3.3.5.2, except that the undepleted wave has the highest circular frequency. In this case, the integrations of the coupled amplitude equations over (X, Y, Z) lead to

$$P_p(L) = T_p^2 P_p(0), \tag{1.7.3.89}$$

$$P_i(L) = P_s(0)\frac{\omega_i}{\omega_s}\Gamma^2L^2\frac{\sinh^2\{\Gamma^2L^2 - [(\Delta k \cdot L)/2]^2\}^{1/2}}{\Gamma^2L^2 - [(\Delta k \cdot L)/2]^2} \tag{1.7.3.90}$$

and

$$\begin{aligned} P_s(L) &= P_s(0)\left[1 + \frac{\omega_s}{\omega_i}\frac{P_i(L)}{P_s(0)}\right] \\ &= P_s(0)\left(1 + \Gamma^2L^2\frac{\sinh^2\{\Gamma^2L^2 - [(\Delta k \cdot L)/2]^2\}^{1/2}}{\Gamma^2L^2 - [(\Delta k \cdot L)/2]^2}\right) \end{aligned} \tag{1.7.3.91}$$

with $\Delta k = k_p - (k_i + k_s)$ and $\Gamma^2 = [B_i P_p(0)]/w_o^2$, where w_o is the beam radius of the three beams and

$$B_i = \frac{8\pi}{\varepsilon_o c}\frac{2N-1}{N}\frac{d_{\text{eff}}^2}{\lambda_s\lambda_i}\frac{T_s T_p T_i}{n_s n_p n_i}.$$

The units are the same as in equation (1.7.3.42).

Equations (1.7.3.90) and (1.7.3.91) show that both idler and signal powers grow exponentially. So, firstly, the generation of the idler is not detrimental to the signal power, in contrast to DFG ($\omega_s - \omega_p = \omega_i$) and SFG ($\omega_s + \omega_p = \omega_i$), and, secondly, the signal power is amplified. Thus DFG ($\omega_p - \omega_s = \omega_i$) combines two interesting functions: generation at ω_i and amplification at ω_s. The last function is called optical parametric amplification (OPA).

The gain of OPA can be defined as (Harris, 1969)

$$G(L) = \left|\frac{P_s(L)}{P_s(0)} - 1\right|. \qquad (1.7.3.92)$$

For example, Baumgartner & Byer (1979) obtained a gain of about 10 for the amplification of a beam at 0.355 μm by a pump at 1.064 μm in a 5 cm long KH_2PO_4 crystal, with a pump intensity of 28 MW cm^{-2}.

According to (1.7.3.91), for $\Delta k^2 L^2/4 \gg \Gamma^2 L^2$, $\sinh^2(im) \rightarrow -\sin^2(m)$ and so the gain is given by

$$G_{\text{small gain}} \simeq \Gamma^2 L^2 \sin c^2\left(\frac{\Delta k \cdot L}{2}\right). \qquad (1.7.3.93)$$

Formula (1.7.3.93) shows that frequencies can be generated around ω_s. The full gain linewidth of the signal, $\Delta\omega_s$, is defined as the linewidth leading to a maximum phase mismatch $\Delta k = 2\pi/L$. If we assume that the pump wave linewidth is negligible, *i.e.* $\Delta\omega_p = 0$, it follows, by expanding Δk in a Taylor series around ω_i and ω_s, and by only considering the first order, that

$$\left|\Delta\omega_s^{\text{small gain}}\right| = \left|\Delta\omega_i^{\text{small gain}}\right| \simeq (2\pi/Lb) \qquad (1.7.3.94)$$

with $b = [1/v_g(\omega_i)] - [1/v_g(\omega_s)]$, where $v_g(\omega) = \partial\omega/\partial k$ is the group velocity.

This linewidth can be termed intrinsic because it exists even if the pump beam is parallel and has a narrow spectral spread.

For type I, the spectral linewidth of the signal and idler waves is largest at the degeneracy: $b = 0$ because the idler and signal waves have the same polarization and so the same group velocity at degeneracy, *i.e.* $\omega_i = \omega_s = \omega_p/2$. In this case, it is necessary to consider the dispersion of the group velocity $\partial^2\omega/\partial^2 k$ for the calculation of $\Delta\omega_s$ and $\Delta\omega_i$. Note that an increase in the crystal length allows a reduction in the linewidth.

For type II, b is never nil, even at degeneracy.

A parametric amplifier placed inside a resonant cavity constitutes an optical parametric oscillator (OPO) (Harris, 1969; Byer, 1973; Brosnan & Byer, 1979; Yang *et al.*, 1993). In this case, it is not necessary to have an incident signal wave because both signal and idler photons can be generated by spontaneous parametric emission, also called parametric noise or parametric scattering (Louisell *et al.*, 1961): when a laser beam at ω_p propagates in a $\chi^{(2)}$ medium, it is possible for pump photons to spontaneously break down into pairs of lower-energy photons of circular frequencies ω_s and ω_i with the total photon energy conserved for each pair, *i.e* $\omega_s + \omega_i = \omega_p$. The pairs of generated waves for which the phase-matching condition is satisfied are the only ones to be efficiently coupled by the nonlinear medium. The OPO can be singly resonant (SROPO) at ω_s or ω_i (Yang *et al.*, 1993; Chung & Siegman, 1993), doubly resonant (DROPO) at both ω_s and ω_i (Yang *et al.*, 1993; Breitenbach *et al.*, 1995) or triply resonant (TROPO) (Debuisschert *et al.*, 1993; Scheidt *et al.*, 1995). Two main techniques for the pump injection exist: the pump can propagate through the cavity mirrors, which allows the smallest cavity length; for continuous waves or pulsed waves with a pulsed duration greater than 1 ns, it is possible to increase the cavity length in order to put two 45° mirrors in the cavity for the pump, as shown in Fig. 1.7.3.18. This second technique allows us to use simpler mirror coatings because they are not illuminated by the strong pump beam.

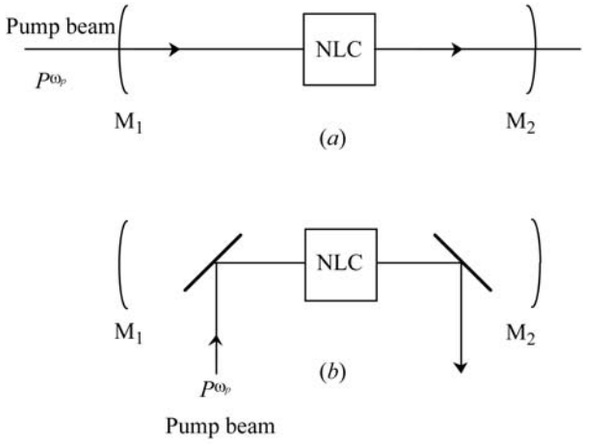

Fig. 1.7.3.18. Schematic OPO configurations. P^{ω_p} is the pump power. (*a*) can be a SROPO, DROPO or TROPO and (*b*) can be a SROPO or DROPO, according to the reflectivity of the cavity mirrors (M_1, M_2).

The only requirement for making an oscillator is that the parametric gain exceeds the losses of the resonator. The minimum intensity above which the OPO has to be pumped for an oscillation is termed the threshold oscillation intensity I_{th}. The oscillation threshold decreases when the number of resonant frequencies increases: $I_{\text{th}}^{\omega_p}$(SROPO) > $I_{\text{th}}^{\omega_p}$(DROPO) > $I_{\text{th}}^{\omega_p}$(TROPO); on the other hand the instability increases because the condition of simultaneous resonance is critical.

The oscillation threshold of a SROPO or DROPO can be decreased by reflecting the pump from the output coupling mirror M_2 in configuration (*a*) of Fig. 1.7.3.18 (Marshall & Kaz, 1993). It is necessary to pump an OPO by a beam with a smooth optical profile because hot spots could damage all the optical components in the OPO, including mirrors and nonlinear crystals. A very high beam quality is required with regard to other parameters such as the spectral bandwidth, the pointing stability, the divergence and the pulse duration.

The intensity threshold is calculated by assuming that the pump beam is undepleted. For a phase-matched SROPO, resonant at ω_s or ω_i, and for nanosecond pulsed beams with intensities that are assumed to be constant over one single pass, $I_{\text{th}}^{\omega_p}$ is given by

$$I_{\text{th}}^{\omega_p} = \frac{1.8}{KL^2(1+\gamma)^2}\left\{\frac{25L}{c\tau} + 2\alpha L + Ln\left[\frac{1}{(1-T)^{1/2}}\right] + Ln(2)\right\}^2. \qquad (1.7.3.95)$$

$K = (\omega_s\omega_i\chi_{\text{eff}}^2)/[2n(\omega_s)n(\omega_i)n(\omega_p)\varepsilon_o c^3]$; L is the crystal length; γ is the ratio of the backward to the forward pump intensity; τ is the $1/e^2$ half width duration of the pump beam pulse; and 2α and T are the linear absorption and transmission coefficients at the circular frequency of the resonant wave ω_s or ω_i. In the nanosecond regime, typical values of $I_{\text{th}}^{\omega_p}$ are in the range 10–100 MW cm^{-2}.

(1.7.3.95) shows that a small threshold is achieved for long crystal lengths, high effective coefficient and for weak linear losses at the resonant frequency. The pump intensity threshold must be less than the optical damage threshold of the nonlinear crystal, including surface and bulk, and of the dielectric coating of any optical component of the OPO. For example, a SROPO using an 8 mm long $KNbO_3$ crystal ($d_{\text{eff}} \simeq 10$ pm V^{-1}) as a nonlinear crystal was performed with a pump threshold intensity of 65 MW cm^{-2} (Unschel *et al.*, 1995): the 3 mm-diameter pump beam was a 10 Hz injection-seeded single-longitudinal-mode Nd:YAG laser at 1.064 μm with a 9 ns pulse of 100 mJ; the SROPO was pumped as in Fig. 1.7.3.18(*a*) with a cavity length of 12 mm, a mirror M_1 reflecting 100% at the signal, from 1.4 to

2 μm, and a coupling mirror M_2 reflecting 90% at the signal and transmitting 100% at the idler, from 2 to 4 μm.

For increasing pump powers above the oscillation threshold, the idler and signal powers grow with a possible depletion of the pump.

The total signal or idler conversion efficiency from the pump depends on the device design and pump source. The greatest values are obtained with pulsed beams. As an example, 70% peak power conversion efficiency and 65% energy conversion of the pump to both signal (λ_s = 1.61 μm) and idler (λ_i = 3.14 μm) outputs were obtained in a SROPO using a 20 mm long KTP crystal ($d_{\rm eff}$ = 2.7 pm V^{-1}) pumped by an Nd:YAG laser (λ_p = 1.064 μm) for eye-safe source applications (Marshall & Kaz, 1993): the configuration is the same as in Fig. 1.7.3.18(*a*) where M_1 has high reflection at 1.61 μm and high transmission at 1.064 μm, and M_2 has high reflection at 1.064 μm and a 10% transmission coefficient at 1.61 μm; the Q-switched pump laser produces a 15 ns pulse duration (full width at half maximum), giving a focal intensity around 8 MW cm^{-2} per mJ of pulse energy; the energy conversion efficiency from the pump relative to the signal alone was estimated to be 44%.

OPOs can operate in the continuous-wave (cw) or pulsed regimes. Because the threshold intensity is generally high for the usual nonlinear materials, the cw regime requires the use of DROPO or TROPO configurations. However, cw-SROPO can run when the OPO is placed within the pump-laser cavity (Ebrahimzadeh *et al.*, 1999). The SROPO in the classical external pumping configuration, which leads to the most practical devices, runs very well with a pulsed pump beam, *i.e.* Q-switched laser running in the nanosecond regime and mode-locked laser emitting picosecond or femtosecond pulses. For nanosecond operation, the optical parametric oscillation is ensured by the same pulse, because several cavity round trips of the pump are allowed during the pulse duration. It is not possible in the ultrafast regimes (picosecond or femtosecond). In these cases, it is necessary to use synchronous pumping: the round-trip transit time in the OPO cavity is taken to be equal to the repetition period of the pump pulse train, so that the resonating wave pulse is amplified by successive pump pulses [see for example Ruffing *et al.* (1998) and Reid *et al.* (1998)].

OPOs are used for the generation of a fixed wavelength, idler or signal, but have potential for continuous wavelength tuning over a broad range, from the near UV to the mid-IR. The tuning is based on the dispersion of the refractive indices with the wavelength, the direction of propagation, the temperature or any other variable of dispersion. More particularly, the crystal must be phase-matched for DFG over the widest spectral range for a reasonable variation of the dispersion parameter to be used. Several methods are used: variation of the pump wavelength at a fixed direction, fixed temperature *etc.*; rotation of the crystal at a fixed pump wavelength, fixed temperature *etc.*; or variation of the crystal temperature at a fixed pump wavelength, fixed direction *etc.*

We consider here two of the most frequently encountered methods at present: for birefringence phase matching, angle tuning and pump-wavelength tuning; and the case of quasi phase matching.

(i) *OPO with angle tuning*.

The function of a tunable OPO is to generate the signal and idler waves over a broad range, $\Delta\omega_s$ and $\Delta\omega_i$, respectively, from a fixed pump wave at ω_p. The spectral shifts $\Delta\omega_s = \omega_s^+ - \omega_s^-$ and $\Delta\omega_i = \omega_i^+ - \omega_i^-$ are obtained by rotating the nonlinear crystal by an angle $\Delta\alpha = \alpha^+ - \alpha^-$ in order to achieve phase matching over the spectral range considered: $\omega_p n(\omega_p, \alpha) = \omega_i n(\omega_i, \alpha) + \omega_s n(\omega_s, \alpha)$ with $\omega_p = \omega_i + \omega_s$ from $(\omega_s^+, \omega_i^-, \alpha^\pm)$ to $(\omega_s^-, \omega_i^+, \alpha^\mp)$, where $(-)$ and $(+)$, respectively, denote the minimum and maximum values of the data considered. Note that $\Delta\omega_s = -\Delta\omega_i$ and so $(\Delta\lambda_i/\lambda_i^+\lambda_i^-) = -(\Delta\lambda_s/\lambda_s^+\lambda_s^-)$ if the spectral bandwidth of the pump, $\delta\omega_p$, is zero.

In the case of parallelepipedal nonlinear crystals, the tuning rate $\Delta\omega_{i,s}/\Delta\alpha$ has to be high because $\Delta\alpha$ cannot exceed about 30° of arc, *i.e.* 15° on either side of the direction normal to the plane surface of the nonlinear crystal: in fact, the refraction can lead to an attenuation of the efficiency of the parametric interaction for larger angles. For this reason, a broad-band OPO necessarily requires angular critical phase matching (CPM) directions over a broad spectral range. However, the angular criticality is detrimental to the spectral stability of the signal and idler waves with regard to the pointing fluctuations of the pump beam: a pointing instability of the order of 100 μrad is considered to be acceptable for OPOs based on KTP or BBO crystals. Fig. 1.7.3.19 shows the phase-matching tuning curves $\lambda_i(\alpha)$ and $\lambda_s(\alpha)$ for (*a*) BBO pumped at λ_p = 355 nm and (*b*) KTP pumped at λ_p = 1064 nm, where $\alpha = \theta$ or φ is an internal angle: the calculations were carried out using the refractive indices given in Kato (1986) for BBO and in Kato (1991) for KTP.

The divergence of the pump beam may increase the spectral bandwidths $\delta\omega_s$ and $\delta\omega_i$: the higher the derivatives $\partial\lambda_{i,s}/\partial\alpha$ are, the higher the spectral bandwidths for a given pump divergence are. Furthermore, $\partial\lambda_{i,s}/\partial\alpha$ vary as a function of the phase-matching angle α. The derivative is a maximum at the degeneracy $\lambda_i = \lambda_s = 2\lambda_p$, when the idler and signal waves are identically polarized: this is the case for BBO as shown in Fig. 1.7.3.19(*a*). We give another example of a type-I BBO OPO pumped at 308 nm by a narrow-band injection-seeded ultraviolet XeCl excimer laser (Ebrahimzadeh *et al.*, 1990): the spectral bandwidth, expressed in cm^{-1} ($\partial\lambda_{i,s}/\lambda_{i,s}^2 = \partial\omega_{i,s}/2\pi c$), varies from $\sim$78 cm^{-1} to $\sim$500 cm^{-1} for a crystal length of 1.2 cm, corresponding to a signal bandwidth $\delta\lambda_s \simeq$ 1.8 nm at 480 nm and $\delta\lambda_s \simeq$ 18 nm at 600 nm, respectively. The degeneracy is not a particular situation with respect to the derivative of the phase-matching curve when the idler and signal waves are orthogonally polarized as shown in Fig. 1.7.3.19(*b*) with the example of KTP.

The way currently used for substantial reduction of the spectral bandwidth is to introduce bandwidth-limiting elements in the OPO cavity, such as a grazing grating associated with a tuning mirror reflecting either the signal or the idler according to the chosen resonant wavelength. The rotations of the nonlinear crystal and of the restricting element have to be synchronized in order to be active over all the wavelength range generated. Narrow bandwidths of about 0.1 cm^{-1} can be obtained in this way, but the gain of such a device is low. High energy and narrow spectral bandwidth can be obtained at the same time by the association of two OPOs: an OPO pumped at ω_p and without a restricting element inside the cavity is seeded by the idler or signal beam emitted by a narrow spectral bandwidth OPO also pumped at ω_p.

The disadvantages of parallelepipedal crystals can be circumvented by using a nonlinear crystal cut as a cylindrical plate, with the cylinder axis orthogonal to the OPO cavity axis and to the plane of the useful phase-matching directions (Boulanger *et al.*, 1999; Pacaud *et al.*, 2000; Fève, Pacaud *et al.*, 2002). Such a geometry allows us to consider any phase-matching range by rotation of the cylinder around its revolution axis. It is then possible to use interactions with a weak angular tuning rate to reduce the spectral bandwidth and increase the stability of the generated beams. Moreover, the propagation of the beams is at normal incidence for any direction, so collinear phase matching can be maintained, leading to better spatial and spectral transverse profiles. Because of the cylindrical geometry of the nonlinear crystal, it is necessary to focus the pump beam and to collect the signal and idler beams with cylindrical lenses. The cavity mirrors, plane or cylindrical, are then placed between the nonlinear crystal and the lenses. The diameter of the crystal being about a few tenths of a millimetre, the associated focal distance is short, *i.e.* a few millimetres, which leads to a strong spatial filtering effect, preventing the oscillation of beams with a quality factor M^2 bigger than about 1.5.

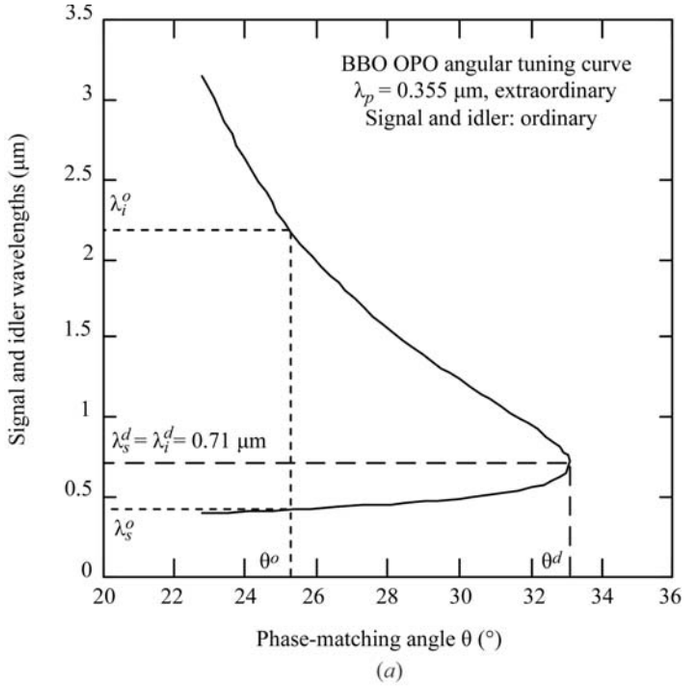

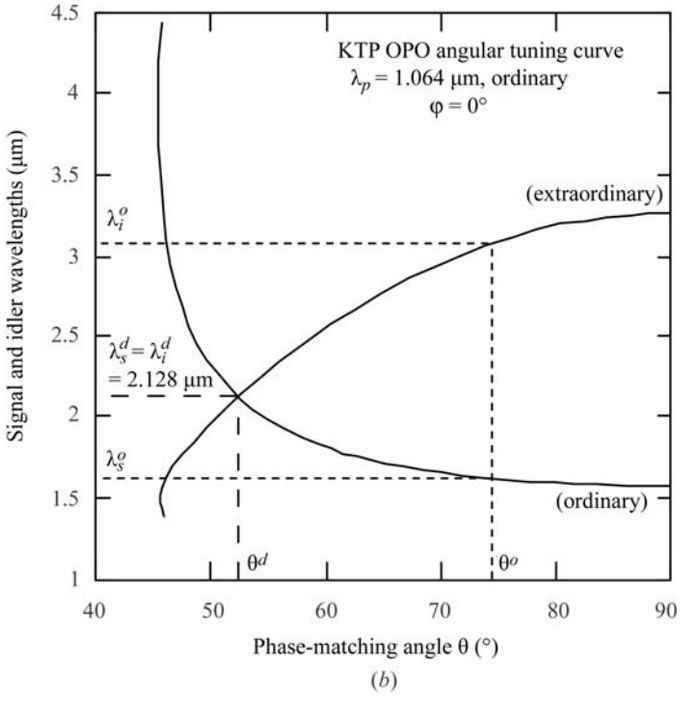

Fig. 1.7.3.19. Calculated angular tuning curves. θ and φ are the spherical coordinates of the phase-matching directions. θ^d is the phase-matching angle of the degeneracy process ($\lambda_i^d = \lambda_s^d = 2\lambda_p$). λ_i^o and λ_s^o are the idler and signal wavelengths, respectively, generated at θ^o. Ordinary and extraordinary refer to the polarization.

(ii) *OPO with a tuning pump*.

The nonlinear crystal is fixed and the pump frequency can vary over $\Delta\omega_p$, leading to a variation of the signal and idler frequencies such that $\Delta\omega_i + \Delta\omega_s = \Delta\omega_p$.

In Fig. 1.7.3.20, the example of *N*-(4-nitrophenyl)-L-propinol (NPP) pumped between 610 and 621 nm is shown (Ledoux *et al.*, 1990; Khodja *et al.*, 1995*a*). The phase-matching curve $\lambda_{i,s}(\lambda_p)$ is calculated from the Sellmeier equations of Ledoux *et al.* (1990) for the case of identical polarizations for the signal and idler waves. The tuning rate is a maximum at the degeneracy, as for angular tuning with identical polarizations.

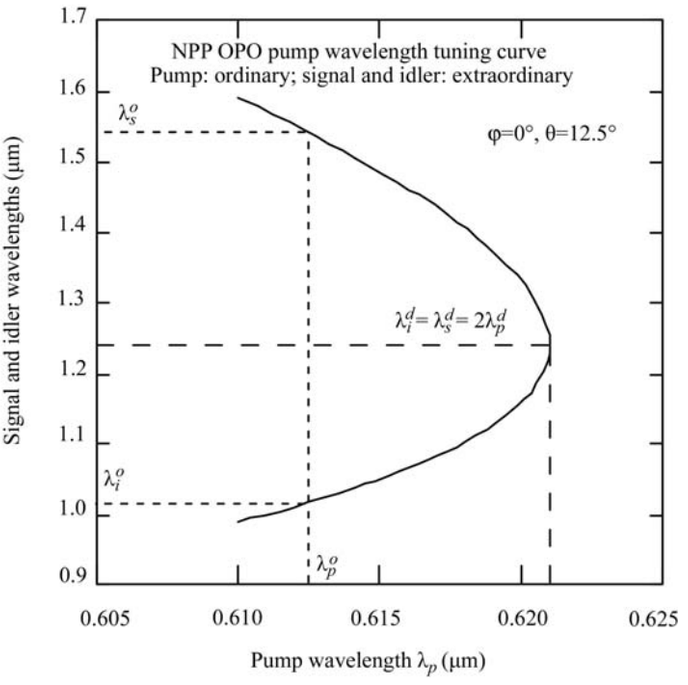

Fig. 1.7.3.20. Calculated pump wavelength tuning curve. λ_p^d is the pump wavelength leading to degeneracy for the direction considered ($\theta = 12.5$, $\varphi = 0°$). Ordinary and extraordinary refer to the polarization.

For any configuration of polarization, the most favourable direction of propagation of an OPO with a tuning pump is a principal axis of the index surface, because the phase matching is angular non-critical and so wavelength critical. In this optimal situation, the OPO has a low sensitivity to the divergence and pointing stability of the pump beam; furthermore, the walk-off angle is nil, which provides a higher conversion efficiency.

(iii) *Quasi-phase-matched OPO with a tunable periodicity*.

In a QPM device, the interacting frequencies are fixed by the frequency dispersion of the birefringence of the nonlinear material and by the periodicity of the grating. A first possibility is to fabricate a series of gratings with different periodicities in the same nonlinear crystal; the translation of this crystal with respect to the fixed pump beam allows us to address the different gratings and thus to generate different couples (ω_s, ω_i). Because the tuning is obtained in discrete steps, it is necessary to combine temperature or angle tuning with the translation of the sample in order to interpolate smoothly between the steps. For example, a device based on a periodically poled $LiNbO_3$ (ppLN) crystal with a thickness of 0.5 mm and a length along the periodicity vector of 1 cm has been developed (Myers *et al.*, 1996). A total of 25 gratings with periods between 26 and 32 μm were realized in 0.25 μm increments. The OPO was pumped at 1.064 μm and generated a signal between 1.35 and 1.98 μm, with the corresponding idler between 4.83 and 2.30 μm.

Fan-shaped gratings have been demonstrated as an alternative approach for continuous tuning (Powers *et al.*, 1998). However, such a structure has the disadvantage of introducing large spectral heterogeneity to the generated beams, because the grating period is not constant over the pump beam diameter.

Finally, the most satisfactory alternative for continuous tuning is the use of a cylindrical crystal with one single grating (Fève *et al.*, 2001). The variations of the signal and idler wavelengths are then obtained by rotation of the cylinder around its revolution axis, which is orthogonal to the OPO cavity axis and to the plane containing the frame vector Λ. For a direction of propagation making an angle α with Λ, the effective period of the grating as seen by the collinear interacting wavevectors is $\Lambda_\alpha = (\Lambda/\cos\alpha)$, leading to a continuous spectral tuning. For example, a rotation over an α range of 26° of a ppKTP cylinder pumped at 1064 nm

leads to a signal tuning range of 520 nm, between 1515 and 2040 nm, while the corresponding idler is tuned over 1340 nm, between 2220 and 3560 nm.

For an overview of OPO and OPA, the reader may refer to the following special issues of the *Journal of the Optical Society of America B*: (1993), **10**(9), 1656–1794; (1993), **10**(11), 2148–2239 and (1995), **12**(11), 2084–2310; and to the *Handbook of Optics* devoted to OPO (Ebrahimzadeh & Dunn, 2000).

1.7.4. Determination of basic nonlinear parameters

We review here the different methods that are used for the study of nonlinear crystals.

1.7.4.1. *Phase-matching directions and associated acceptance bandwidths*

The very early stage of crystal growth of a new material usually provides a powder with particle sizes less than 100 μm. It is then impossible to measure the phase-matching loci. Nevertheless, careful SHG experiments performed on high-quality crystalline material may indicate whether the SHG is phase-matched or not by considering the dependence of the SHG intensity on the following parameters: the angle between the detector and the direction of the incident fundamental beam, the powder layer thickness, the average particle size and the laser beam diameter (Kurtz & Perry, 1968). However, powder measurements are essentially used for the detection in a simple and quick way of noncentrosymmetry of crystals, this criterion being necessary to have a nonzero $\chi^{(2)}$ tensor (Kurtz & Dougherty, 1978). They also allow, for example, the measurement of the temperature of a possible centrosymmetric/noncentrosymmetric transition (Marnier *et al.*, 1989).

For crystal sizes greater than few hundred μm, it is possible to perform direct measurements of phase-matching directions. The methods developed at present are based on the use of a single crystal ground into an ellipsoidal (Velsko, 1989) or spherical shape (Marnier & Boulanger, 1989; Boulanger, 1989; Boulanger *et al.*, 1998); a sphere is difficult to obtain for sample diameters less than 2 mm, but it is the best geometry for large numbers and accurate measurements because of normal refraction for every chosen direction of propagation. The sample is oriented using X-rays, placed at the centre of an Euler circle and illuminated with fixed and appropriately focused laser beams. The experiments are usually performed with SHG of different fundamental wavelengths. The sample is rotated in order to propagate the fundamental beam in different directions: a phase-matching direction is then detected when the SHG conversion efficiency is a maximum. It is then possible to describe the whole phase-matching cone with an accuracy of 1°. A spherical crystal also allows easy measurement of the walk-off angle of each of the waves (Boulanger *et al.*, 1998). It is also possible to perform a precise observation and study of the internal conical refraction in biaxial crystals, which leads to the determination of the optic axis angle $V(\omega)$, given by relation (1.7.3.14), for different frequencies (Fève *et al.*, 1994).

Phase-matching relations are often poorly calculated when using refractive indices determined by the prism method or by measurement of the critical angle of total reflection. Indeed, all the refractive indices concerned have to be measured with an accuracy of 10^{-4} in order to calculate the phase-matching angles with a precision of about 1°. Such accuracies can be reached in the visible spectrum, but it is more difficult for infrared wavelengths. Furthermore, it is difficult to cut a prism of few mm size with plane faces.

If the refractive indices are known with the required accuracy at several wavelengths well distributed across the transparency region, it is possible to fit the data with a Sellmeier equation of the following type, for example:

$$n_i^2(\lambda) = A_i + \frac{B_i\lambda^2}{\lambda^2 - C_i} + D_i\lambda^2. \qquad (1.7.4.1)$$

n_i is the principal refractive index, where $i = o$ (ordinary) and e (extraordinary) for uniaxial crystals and $i = x$, y and z for biaxial crystals.

It is then easy to calculate the phase-matching angles (θ_{PM}, φ_{PM}) from (1.7.4.1) using equations (1.7.3.27) or (1.7.3.29) where the angular variation of the refractive indices is given by equation (1.7.3.6).

The measurement of the variation of intensity of the generated beam as a function of the angle of incidence can be performed on a sphere or slab, leading, respectively, to internal and external angular acceptances. The thermal acceptance is usually measured on a slab which is heated or cooled during the frequency conversion process. The spectral acceptance is not often measured, but essentially calculated from Sellmeier equations (1.7.4.1) and the expansion of Δk in the Taylor series (1.7.3.43) with $\xi = \lambda$.

1.7.4.2. *Nonlinear coefficients*

The knowledge of the absolute magnitude and of the relative sign of the independent elements of the tensors $\chi^{(2)}$ and $\chi^{(3)}$ is of prime importance not only for the qualification of a new crystal, but also for the fundamental engineering of nonlinear optical materials in connection with microscopic aspects.

However, disparities in the published values of the nonlinear coefficients of the same crystal exist, even if it is a well known material that has been used for a long time in efficient devices (Eckardt & Byer, 1991; Boulanger, Fève *et al.*, 1994). The disagreement between the different absolute magnitudes is sometimes a result of variation in the quality of the crystals, but mainly arises from differences in the measurement techniques. Furthermore, a considerable amount of confusion exists as a consequence of the difference between the conventions taken for the relation between the induced nonlinear polarization and the nonlinear susceptibility, as explained in Section 1.7.2.1.4.

Accurate measurements require mm-size crystals with high optical quality of both surface and bulk.

1.7.4.2.1. *Non-phase-matched interaction method*

The main techniques used are based on non-phase-matched SHG and THG performed in several samples cut in different directions. The classical method, termed the Maker-fringes technique (Jerphagnon & Kurtz, 1970; Herman & Hayden, 1995), consists of the measurement of the harmonic power as a function of the angle between the fundamental laser beam and the rotated slab sample, as shown in Fig. 1.7.4.1(*a*).

The conversion efficiency is weak because the interaction is non-phase-matched. In normal incidence, the waves are collinear and so formulae (1.7.3.42) for SHG and (1.7.3.80) for THG are valid. These can be written in a more convenient form where the coherence length appears:

$$\begin{aligned} P^{n\omega}(L) &= A^{n\omega}[P^{\omega}(0)]^n (d_{\text{eff}}^{n\omega} \cdot l_c^{n\omega})^2 \sin^2(\pi L/2l_c^{n\omega}) \\ l_c^{2\omega} &= (\pi c/\omega)(2n_3^{2\omega} - n_1^{\omega} - n_2^{\omega})^{-1} \\ l_c^{3\omega} &= (\pi c/\omega)(3n_4^{3\omega} - n_1^{\omega} - n_2^{\omega} - n_3^{\omega})^{-1}. \end{aligned} \qquad (1.7.4.2)$$

The coefficient $A^{n\omega}$ depends on the refractive indices in the direction of propagation and on the fundamental beam geometry: $A^{2\omega}$ and $A^{3\omega}$ can be easily expressed by identifying (1.7.4.2) with (1.7.3.42) and (1.7.3.80), respectively.

When the crystal is rotated, the harmonic and fundamental waves are refracted with different angles, which leads to a variation of the coherence length and consequently to an oscillation of the harmonic power as a function of the angle of incidence, α, of the fundamental beam. Note that the oscillation